

# Australian Journal of Earth Sciences

An International Geoscience Journal of the Geological Society of Australia

ISSN: (Print) (Online) Journal homepage: <https://www.tandfonline.com/loi/taje20>

## The pollen record from marine core MD03-2607 from offshore Kangaroo Island spanning the last 125 ka; implications for vegetation changes across the Murray-Darling Basin

P. De Deckker, S. van der Kaars, S. Haberle, Q. Hua & J.-B. W. Stuut

To cite this article: P. De Deckker, S. van der Kaars, S. Haberle, Q. Hua & J.-B. W. Stuut (2021): The pollen record from marine core MD03-2607 from offshore Kangaroo Island spanning the last 125 ka; implications for vegetation changes across the Murray-Darling Basin, Australian Journal of Earth Sciences, DOI: [10.1080/08120099.2021.1896578](https://doi.org/10.1080/08120099.2021.1896578)

To link to this article: <https://doi.org/10.1080/08120099.2021.1896578>

 View supplementary material 

 Published online: 28 Mar 2021.

 Submit your article to this journal 

 View related articles 

 View Crossmark data 

# The pollen record from marine core MD03-2607 from offshore Kangaroo Island spanning the last 125 ka; implications for vegetation changes across the Murray-Darling Basin

P. De Deckker<sup>a</sup> , S. van der Kaars<sup>b,c</sup> , S. Haberle<sup>d,e</sup> , Q. Hua<sup>f</sup>  and J.-B. W. Stuut<sup>g</sup> 

<sup>a</sup>Research School of Earth Sciences, The Australian National University, Canberra, Australia; <sup>b</sup>School of Earth, Atmosphere and Environment, Monash University, Clayton, Australia; <sup>c</sup>Department of Earth Sciences, Vrije Universiteit Amsterdam, Amsterdam, The Netherlands; <sup>d</sup>School of Culture, History and Language, The Australian National University, Canberra, Australia; <sup>e</sup>ARC Centre of Excellence for Australian Biodiversity and Heritage, The Australian National University, Canberra, Australia; <sup>f</sup>Australian Nuclear Science and Technology Organisation, Lucas Heights, Australia; <sup>g</sup>NIOZ—Royal Netherlands Institute for Sea Research, and Utrecht University, Texel, The Netherlands

## ABSTRACT

A palynological record spanning the last glacial–interglacial period was derived from high-resolution, deep-sea core MD03-2607, located near Kangaroo Island in South Australia. The core site lies opposite the mouth of the River Murray that, together with the Darling River, drains the extensive ( $\sim 1.6 \times 10^6 \text{ km}^2$ ) Murray-Darling Basin (MDB). The record comprises 120 samples and is compared with detailed records of sea-surface temperature (SST), the  $C_3/C_4$  plant ratio obtained from the  $\delta^{13}C$  of *n*-alkanes from leaf waxes, the fluvial clay fraction and its neodymium isotopic composition, airborne dust and the biomass-burning component levoglucosan. The chronology of the core is robust; it is built on 24 radiocarbon dates derived from planktic foraminifera, 16 optically stimulated luminescence dates, plus 12 tie points linked to the astronomically tuned marine isotopic record. Algal remains are found in nearly all samples supporting our postulation that the palynoflora is predominantly waterborne. Major findings are that the gymnosperm *Callitris*, together with high percentages of herb pollen (mostly  $C_3$  plants), is predominant during cold, arid phases, whereas *Eucalyptus*, is predominant during warmer and wetter periods. High charcoal concentration coincides with high percentages of *Eucalyptus*, mostly during wet and warm periods. Using the geochemistry of the core's fluvial sediments, it has been possible to identify when water-transported palynoflora and charcoal originated from the Murray sub-basin (consisting of the River Murray and its main tributaries but not from central or western South Australia). During those periods, rainfall principally originated from the southeastern Indian Ocean. When the Darling sub-basin was the main source of the palynoflora, rainfall must have instead originated from northern Australia. The eolian dust record from the core shows that the dust signal generally coincides with the increased values in herb pollen, in particular during the Last Glacial Maximum (LGM) when, in addition to high herb percentages, *Callitris* representation also increased. This dry landscape taxon likely colonised the then-exposed Lacedpede Shelf during this period of extreme low sea-level. There is a good correspondence between SST and mean annual precipitation reconstructed from the pollen counts. During warm phases in the ocean, *Eucalyptus* was the dominant tree taxon, especially for the entirety of Marine Isotope Stages (MIS) 5, plus MIS 3 and MIS 1. Charcoal levels were particularly low during the dry phases MIS 4 and 2, and even more so during the LGM.

## KEY POINTS

1. We provide a very detailed pollen diagram from a deep-sea core taken offshore from the mouth of the River Murray.
2. This record details vegetation changes in the Murray-Darling Basin spanning the last glacial/interglacial cycle.
3. The pollen record is compared with other proxies obtained from the marine core, such as sea-surface temperature, changes in  $C_3/C_4$  plants percentages, geochemical analyses of terrigenous sediments that inform on the origin of the sediments reaching the ocean and by implication the origin of the pollen.

## ARTICLE HISTORY

Received 12 December 2020  
Accepted 19 February 2021

## KEYWORDS

last glacial/interglacial cycle; Murray-Darling basin; Lacedpede Shelf; *Gyrostemon*; *Callitris*;  $C_3/C_4$  plants; charcoal; levoglucosan; airborne dust; fluvial muds; neodymium isotopes; Ti/Ca

- Charcoal counts obtained from the core are compared with the pollen spectra and clearly indicate the large incidence of fires during wet and warm periods when *Eucalyptus* pollen was abundant. Low charcoal counts occur during dry and cold phases when *Callitris* pollen were predominant over *Eucalyptus*.

## Introduction

There is a lack of high-resolution studies on vegetation changes in Australia spanning the last few glacial/interglacial cycles that are well dated and can be directly compared with long records constructed from other paleoenvironmental proxies, especially those indicative of climatic changes. The reason is that many depocentres such as lakes and marshes from which pollen and spores are obtained frequently suffer deflation (such as the case of playa lakes), and pollen can undergo diagenesis (resulting from oxygenation and changes in alkalinity levels) and, in the case of marshes, pollen can percolate through the commonly porous fibrous material. In addition, many continental pollen sequences suffer from a lack of suitable materials to establish reliable chronologies for sequences older than the radiocarbon dating limit. The optically stimulated luminescence (OSL) dating technique now offers a new outlook on older sequences, but the technique suffers from somewhat large error bars, extending up to several millennia for old sequences.

Vegetation records from deep-sea cores, which commonly have a continuous deposition of sediments, can also be compared with other marine proxies such as sea-surface temperature (SST) signals. These sequences can be precisely dated by oxygen-isotope stratigraphies based on the composition of foraminifera linked to global chronologies (tuned to astronomical ages), enabling chronological control well beyond the limits of radiocarbon dating. In addition, other continental proxies obtained from the same core such as airborne dust, river clays and their geochemical composition, can be compared against the pollen record to better define environmental changes both on land and at sea.

Deep-sea core MD03-2607, located offshore the River Murray mouth close to Kangaroo Island, offshore South Australia (Figure 1), provided 13.5 m of uninterrupted sedimentation that spans 125 000 years. Already there have been several studies carried out on the core, including detailed SST (Lopes dos Santos De Deckker, Sinninghe, et al., 2013), stable-isotope stratigraphy (De Deckker, Arnold, et al., 2019; Gingele & De Deckker, 2005a), geochemistry of the clay-size sediment fraction (Gingele et al., 2004), organic geochemical analyses such *n*-alkanes (Lopes dos Santos, De Deckker, Hopmans, et al., 2013) and the presence of the biomass-burning marker levoglucosan (Lopes dos Santos, Spooner, et al., 2013). In this paper, we present, a detailed study of pollen, spores and charcoal that we compare with these existing studies.

## Environmental setting

### *Lacepede Shelf and River Murray paleomeanders*

The Lacepede Shelf, which is extension seaway of the Murray-Darling Basin (MDB) that exits to the sea via the present-day Murray Mouth, is an extensive embayment that covers approximately  $20 \times 10^3 \text{ km}^2$  and is some 180 km wide (Figures 1 and 2). It is bordered by Kangaroo Island and the Fleurieu Peninsula to the west and Youngusband Peninsula and adjacent Coorong Lagoon to the north and it extends as far as Cape Jaffa to the east (Figure 1). The shelf extends as far as the edge of the continental shelf that is bordered in places by a fairly narrow continental slope. Elsewhere, it is bordered by a series of deep-sea canyons, which together are coined the Murray Canyons Group, with the well-researched Sprigg Canyon (Hill et al., 2005; Sprigg, 1947; von der Borch, 1968) that extends down to the abyssal plain, some 4.5 km at its base. The canyons are believed to be still active (Supplemental material, Figure S1). For further information on the Lacepede Shelf, refer to James and Bone (2011).

Extensive bathymetric and seismic survey work conducted in 2005 and 2006 using the *RV Southern Surveyor* revealed the ancient courses of the River Murray that were formed when the Lacepede Shelf was exposed during the frequent periods of low sea-level (Hill et al., 2009). It was found that the paleomeanders served as conduits of fluvial sediments over the Lacepede Shelf, onto the continental slope and into the Murray Canyons Group (Hill et al., 2009). Hence, it is the case that deep-sea cores taken on the continental slope in this location do record a mixture of fluvial sediments transported seaward together with pelagic (marine) sediments and organisms (such as foraminifera and calcareous nanoplankton), thus offering the potential to determine events that occurred on land and in the sea at the same time. Two cores (MD03-2607 and MD03-2611) were obtained in 2003 using the *RV Marion Dufresne* and have been the focus of numerous studies that have all indicated the exemplary degree of preservation of materials within these archives for paleoenvironmental reconstructions. These will be discussed in the sections below. The current paper deals with the record from MD03-2607 core.

### *Regional description of the Murray-Darling Basin*

It is useful to provide an overview of the MDB with respect to its present-day (*viz.* pre-European arrival) vegetation and meteorological conditions. The MDB is a very large inland basin that covers some  $1.6 \times 10^6 \text{ km}^2$  and discharges into

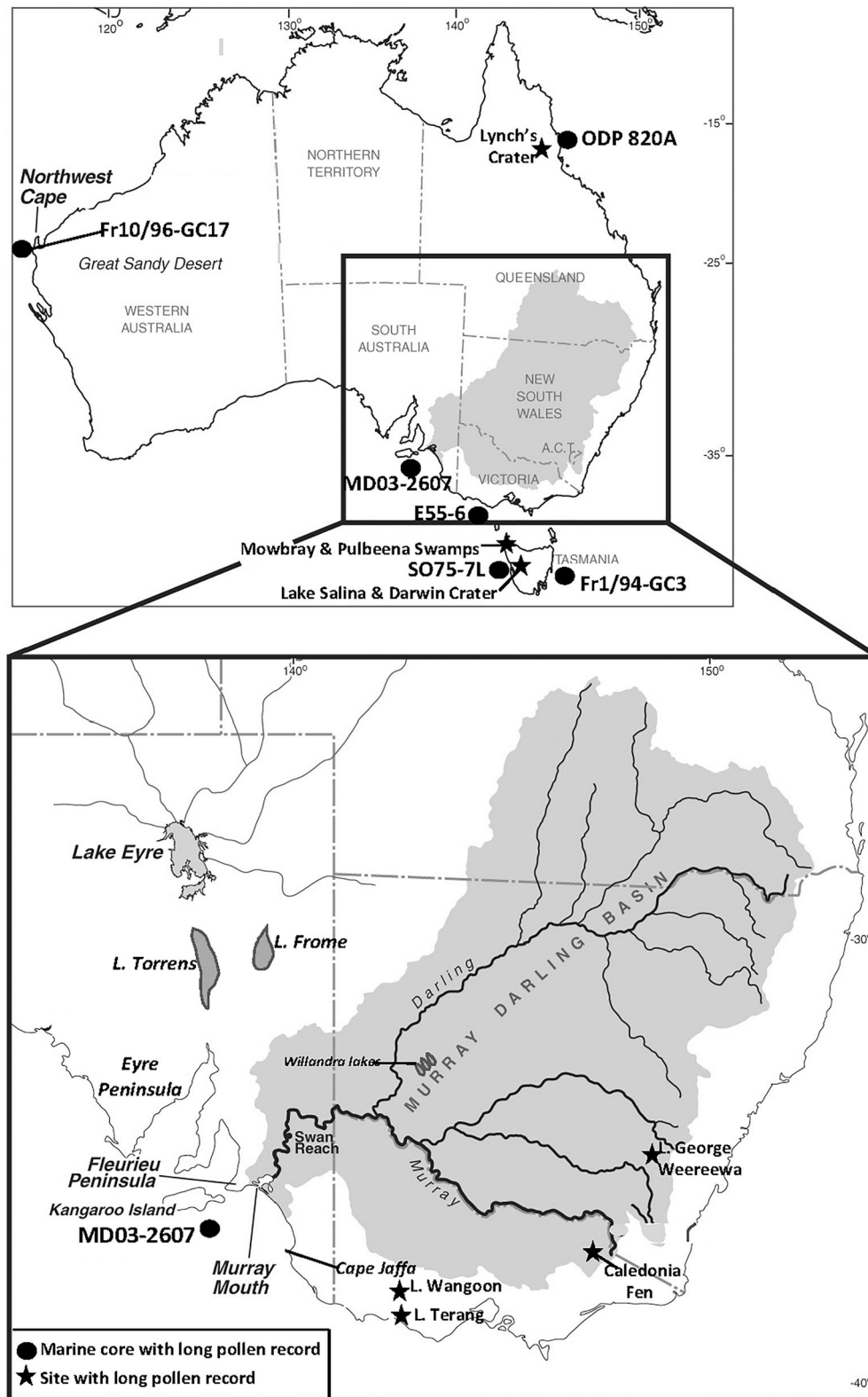


Figure 1. Map of Australia showing the extent of the vast Murray-Darling Basin (MDB) in shaded grey and the location of the deep-sea cores (black circles) as well as the long pollen sequences recovered on land (stars), all discussed in this study. The enlargement shows the major rivers in the MDB as well as major playa lakes in central South Australia.

the sea at the Murray Mouth in southeast South Australia (Figure 1). It consists of two major rivers with numerous tributaries: the Darling River in the northern and western

region (referred to here as the Darling sub-basin) and the River Murray in the eastern and southern region (referred to here as the Murray sub-basin). The latter drains the

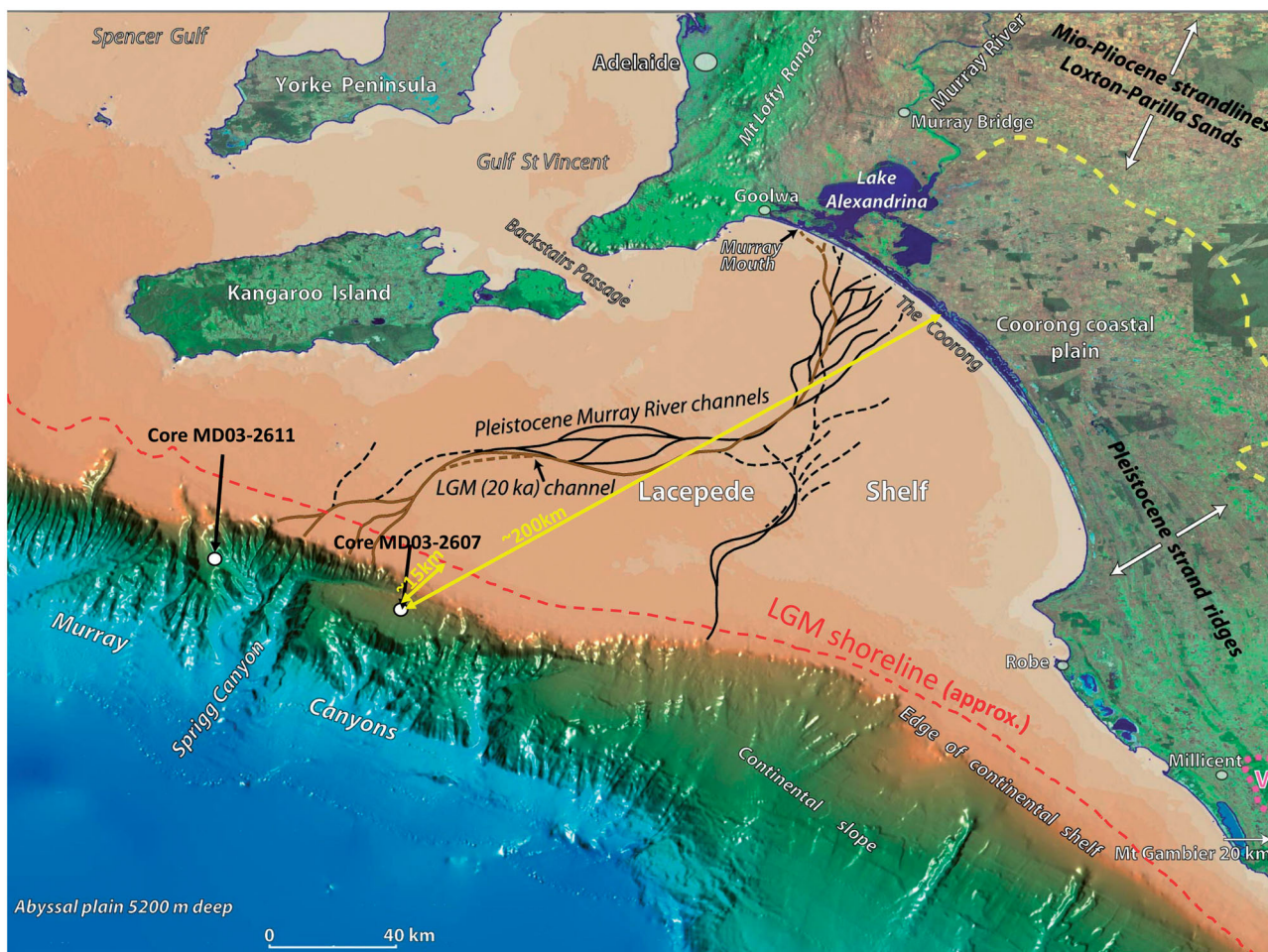


Figure 2. Sketch providing a tilted view of the Lacepede Shelf down to the abyss shown in deep blue, and the location of the two deep-sea cores discussed in this paper that are at opposite ends of the Murray Canyons Group and are on almost horizontal platforms not subject to turbidity currents that are so common in canyons region. Note that both cores occur opposite of some of the ancient meanders of the River Murray (shown in black, and brown for the Last Glacial Maximum [LGM]) that would have been active during periods of low sea-level. MD03-2607 is located today some 200 km from the Murray Mouth, but during the LGM, it would only be 15 km from the edge of the continent (approximate red dotted line). Map modified from Hill *et al.* (2009).

eastern highlands and today receives most of its rainfall, which originates from the Southern Ocean, with some from the Tasman Sea, during the austral winter. On average, the Murray sub-basin receives 200 to 400 mm precipitation per year, but climatic conditions vary greatly from year to year. By contrast, the Darling River catchment receives most of its rainfall, which originates to a large extent from the northern part of the continent, during the austral summer. On average, rainfall for this sub-basin is much higher, ranging from 400 to 800 mm precipitation, with extremes going down to 300 mm and well over 1200 mm in the highlands. Nonetheless, the upper portion of the basin encompasses the semiarid zone of Australia and this is reflected by the vegetation present with the characteristic flora of the Darling catchment consisting predominantly of open shrubland, chenopods and grasses with some woodland. The dominant taxa are *Acacia* and *Casuarina* spp., which may include *Casuarina* and *Allocasuarina* and even *Gymnostoma* pollen. The Murray sub-basin is characterised by woodland and open forest with *Eucalyptus* spp. the dominant trees. Riparian vegetation is also an important

source for waterborne pollen as these communities, commonly dominated by *Eucalyptus* spp. (e.g. river red gums and black box), may act as refugia for drought-intolerant species during drier climate episodes. In the montane regions, pteridophyte taxa are also a significant component of the vegetation community.

### Previous work on MD03-2607 of relevance to its pollen record

#### Description of Calypso core MD03-2607

MD03-2607 core was taken on 21 February 2003 with the RV *Marion Dufresne* during the AUSCAN campaign (Hill & De Deckker, 2004) on a flat platform east of Sprigg Canyon (Figure 1; Supplemental material, Figures S1 and S2) south-east of Kangaroo Island. Its location is 36°57.64' S, 137°E24.39', and it was taken at 865 m water depth. The core is 32.95 m long, with the upper 13.5 m (of interest here) consisting of massively bedded fine to very fine (foraminiferal) sands with minor colour variation from

darker to paler olive-grey. In this upper section of the core, occasional zones of irregular or wavy centimetre-scale darker and lighter layers occur. Below 14.7 m, the sediments are finer in texture.

As already shown by Gingele *et al.* (2004, 2007) and Gingele and De Deckker (2005a), this core contains a record of fluvial clays from the River Murray deposited at sea. It is located close to the edge of the continental shelf and the nature of the sediment will change depending on the proximity of the core site to the continent's edge/shoreline. Based on the Lambeck *et al.* (2014) global sea-level reconstructions, this boundary varied between ~200 km today from the Murray Mouth and approximately 15 km during the lowest sea-level experienced during the Last Glacial Maximum (LGM). This means that during periods of low sea-levels the amount of terrigenous material would have been greater than in periods of sea-level high stands. In fact, colour reflectance of the entire core (following the technique applied by Lourens, 2004, to deep-sea cores from the Mediterranean Sea) carried out on the ship soon after the opening of the cores clearly supported this observation. For additional information, refer to the Supplemental material (Figure S5).

#### **Clay mineralogy and neodymium isotopic ratios**

Following a comprehensive study by Gingele and De Deckker (2005a) of the clay composition at 32 river sites in the MDB from both the River Murray and Darling River and their tributaries, it has been possible to determine the origin of the fluvial clays in the two Murray Canyons Group cores MD03-2607 and MD03-2611. These investigations, in addition to a close scrutiny of the last 17 ka of MD03-2611 by Gingele *et al.* (2007), showed that the fluvial clays deposited varied in origin from within the MDB. Gingele and De Deckker (2005a) also studied the Nd isotopic composition of the clay fraction of those fluvial samples in MD03-2611. Following this work, Bayon *et al.* (2017) studied MD03-2607 and convincingly identified that during the last *ca* 90 000 years the Nd isotopic ratios shifted at times from a Murray sub-basin signal (from 88 to 76 ka BP) to a Darling sub-basin signal until 14 ka BP, and then back to a signal from the Murray sub-basin (this time based on Gingele *et al.*, 2007's work done on MD03-2611). The implications of the shift in river supply from different parts of the MDB caused by rainfall originating at time from the north (via the monsoonal system) or from the Southern Ocean (via oceanic fronts transgressing over southern Australia) will be discussed in this paper.

#### **Planktic foraminifera faunal counts and proxies for SSTs**

Spooner (2005) provided the groundwork on planktic foraminifer counts for MD03-2607 that was later used by Lopes dos Santos, Spooner *et al.* (2013) to estimate SSTs

based on the modern analogue technique, in conjunction with the AUSMAT-F4 database established by Barrows and Juggins (2005). Lopes dos Santos, Spooner *et al.* (2013) also compared those values against other SST proxies ( $U_{37}^{K'}$ ,  $TEX_{86}^H$ , LDI). These will be discussed in this paper.

#### **Oxygen isotopes measured on planktic and benthic foraminifera**

De Deckker, Arnold, *et al.* (2019), Gingele *et al.* (2004), Lopes dos Santos *et al.* (2012), Lopes dos Santos, Spooner *et al.* (2013) and Spooner (2005) all contributed to the analyses of both planktic (*Globigerina bulloides*) and benthic foraminifera (a combination of *Planulina wuellerstorfi* and *Uvigerina* sp.) that provided the basis for a sound and detailed chronology of the last glacial/interglacial portion of MD03-2607 (*viz.* the upper 13.5 m). The benthic foraminiferal isotope record was used by De Deckker, Arnold, *et al.* (2019) to update the chronology for comparison with the standard  $\delta^{18}O$  curve for the Pacific Ocean Intermediate water based the benthic  $\delta^{18}O$  record of Pacific target core MD97-2120 (45.53°S, 174.93°E; 1210 m; Pahnke & Zahn, 2005) located offshore New Zealand (see Lisiecki & Stern, 2016 and discussion in De Deckker, Arnold, *et al.*, 2019) and is further updated here. The chronology based on a total of 23  $^{14}C$  ages obtained from planktic foraminifera is updated based on new estimates of marine reservoir ages. The Lopes dos Santos, Spooner *et al.* (2013) study also relied on 13 OSL dates.

#### **Productivity changes registered in MD03-2607**

Lopes dos Santos *et al.* (2012) assessed primary productivity changes above core site MD03-2607 based on detailed analysis of the  $\delta^{13}C$  of planktic foraminiferal record that showed distinct minima during the two deglaciations recorded in the core as well as for the Marine Isotope Stage 4/3 transition, suggesting tentatively that  $^{13}C$ -depleted Southern Ocean waters reached the coast of southern Australia. In addition, this study suggested that increased primary productivity offshore southeastern Australia was mainly due to stronger westerly winds during glacial periods.

Lopes dos Santos *et al.* (2012) also examined the Diol index in MD03-2607, which is the ratio of long-chain 1,14 diols produced by *Proboscia* diatoms that grow in the early stages of upwelling when nutrient concentrations strongly increase. The Diol index values in MD03-2607 shows maxima during Marine Isotope Stages (MIS) 1, 3 and 5e and minima during deglaciation periods (Lopes dos Santos *et al.*, 2012, figure 3). Disappointingly, despite several attempts, no diatom frustules were recovered from MD03-2607 or MD03-2611, likely resulting from opaline silica dissolution. Quartz grains and sponge spicules were recovered from most samples in both cores.

## Organic compounds to unravel C<sub>3</sub>/C<sub>4</sub> plants and evidence of biomass burning

Lopes dos Santos, De Deckker, Hopmans, *et al.* (2013) examined the stable carbon isotopic composition of higher plant wax *n*-alkanes and levels of biomass burning from the accumulation rates of the biomarker levoglucosan in MD03-2607 spanning the last 135 ka BP. The  $\delta^{13}\text{C}$  of *n*-alkanes plants varied from  $-30$  to  $-26\text{‰}$  VPDB throughout the sampled core, which was converted to the percentage of plants with C<sub>4</sub> carbon fixation pathways that corresponds to a variation from  $\sim 35$  to 70% of C<sub>4</sub> plant contribution. The remarkable feature of the C<sub>3</sub>/C<sub>4</sub> vegetation record was the abrupt drop in % of C<sub>4</sub> from  $>70$  to  $\sim 38\%$  between 44 and 42 ka BP (Lopes dos Santos, De Deckker, Hopmans, *et al.*, 2013, figure 3; the chronology has been revised in this paper). The shift in accumulation rates of levoglucosan, a biomarker exclusively produced during burning of land vegetation and transported by dust and smoke to distant areas where it is preserved in soils and sediments (see references in Lopes dos Santos, De Deckker, Hopmans, *et al.*, 2013) significantly increased at a time when C<sub>4</sub> percentages decreased. Lopes dos Santos, De Deckker, Hopmans, *et al.* (2013) provided a comprehensive discussion on the cause of the extensive fires, which they did not attribute directly to human activity nor to the extinction of the megafauna. It is only at the LGM that levoglucosan levels rose again, but this was not the result of the fact that sea-level was significantly low, with the coast being close to the core site (Figure 2), but instead, being an aerosol, indicating biomass burning in an unknown part of the basin. The other decreases in C<sub>4</sub> plant percentages occurred during both the penultimate glaciation (MIS 6) and the LGM.

### Previous study on MIS 4

De Deckker, Arnold, *et al.* (2019) applied numerous proxies to define in detail the timing and paleoclimatic conditions of MIS 4 recorded in MD03-2607. This period of time that lasted some 11 000 years saw a significant sea-level drop ( $\sim 100$  m at its climax), very low SSTs and significant vegetation changes inland. The core data were compared with other events in the Southern Hemisphere, including glacial advances on the South Island of New Zealand, the Australian mainland and Papua New Guinea. The age control for that episode in the core relied on six additional OSL dates combined with a link to the Lisiecki and Stern (2016)  $\delta^{18}\text{O}$  isotope chronology established for sites bathed by Pacific Intermediate Water (see Supplemental material, Figure S3) as an improvement on the global chronology originally established by Lisiecki and Raymo (2005).

### Long-term pollen record from SE Australia, based on marine cores

The data from five deep-sea cores in the Australian region, considered together, provide a comprehensive pollen

record spanning the last glacial/interglacial cycle or part thereof. These are in order of publication: core SO75-7L located west of Tasmania (van de Geer *et al.*, 1994), core E55-6 offshore Victoria (Harle, 1997), the long ODP 820 core offshore the Great Barrier Reef (Moss & Kershaw, 2000), core Fr10-95/GC17 offshore Northwest Cape, north-western Western Australia (van der Kaars & De Deckker, 2002), and the short but condensed core Fr1-94/GC3 offshore eastern Tasmania (De Deckker, van der Kaars, *et al.*, 2019). The latter spans the last four glacial/interglacial cycles. The core locations are shown in Figure 1, and a summary of the findings obtained from all these cores is presented in the Supplemental material.

The long-term records from inland sequences in Australia are not mentioned here owing to the lack of suitable and continuous chronologies past the radiocarbon record but are briefly referred to below.

## Methods

### Extraction and analysis of pollen, spores and charcoal

A total of 120 samples were analysed for their palynological content, 20 of which had already been processed for the published investigations on Marine Isotope Stage 4 (De Deckker, Arnold, *et al.*, 2019). Samples used in that study were treated in the same manner: 3 cm<sup>3</sup> of sediment was treated with 10% sodium-pyrophosphate and sieved over a 180- $\mu\text{m}$  and 8- $\mu\text{m}$  mesh. The fraction between 180  $\mu\text{m}$  and 8  $\mu\text{m}$  was treated with 10% hydrochloric acid, then acetolysis was undertaken, followed by heavy liquid separation using sodium-polytungstate (s.w. 2.0, for 20 min at 2000 rpm). This last step was repeated twice, the floating residue was dehydrated with 96% ethanol. Slides were mounted with glycerol and sealed with paraffin wax. Sander van der Kaars analysed all the samples and counted on average well over 200 grains, but this ranged from 105 to 431 (Figures 3 and 4j). A known amount of *Lycopodium* marker spores was added to each sample prior to chemical treatment to enable calculation of palynomorph concentrations. Throughout the paper and in figures charcoal concentrations as particles/cm<sup>3</sup>.

### Statistical analysis of the pollen assemblages

End-member modelling: we used the statistical technique provided in the R package EMMAgeo (Dietze & Dietze, 2016, 2019) to decompose the multi-modal pollen distributions into inherent subpopulations, commonly termed end-member modelling analysis. This program was originally applied to sediments, for analyses such as grainsizes, as a tool to infer the underlying sediment sources, transport and (post-)depositional processes (Dietze & Dietze, 2019).

Pollen transfer functions: estimates of annual rainfall for the 120 pollen samples from MD03-2607 were generated using the transfer function developed by Cook and van der



Kaars (2006). Functions were produced in C2 (version 1.7.7) (Juggins, 2013) using the method of weighted averaging partial least-squares regression (WA-PLS) (after Ter Braak & Juggins, 1993) and are based on the square root of the pollen percentage values. In order to test the reliability of the functions, each was cross-validated using the leave-one-out method.

### Dating

A total of 24 samples for AMS radiocarbon dating was used to date the upper 6 m of the core, three of which were obtained for this study. The same section was also dated with some 13 Optical Stimulation Luminescence (OSL) samples. Planktic foraminifera were used for  $^{14}\text{C}$  dating and relevant information is presented in Lopes dos Santos *et al.* (2012), where information on the OSL samples is also available. An additional 6 OSL samples deeper in the core were analysed and information on these is presented in De Deckker, Arnold, *et al.* (2019). Note that one of these samples was an outlier. The depth position of all these samples is shown in Supplemental material (Figure S4).

### XRF-scanning of MD03-2607

A  $2 \times 2$  cm u-channel was taken from the entire core MD03-2607 and elemental composition was obtained following the procedure presented in Stuut *et al.* (2014) using an Avaatech XRF core scanner at 1-cm resolution at the Royal Netherlands Institute for Sea Research (NIOZ).

### Colour reflectance of MD03-2607

Colour reflectance of the entire core (following the technique applied by Lourens, 2004, to deep-sea cores in the Mediterranean Sea) was carried out on the ship soon after the opening of the cores using a Minolta CM-508 spectrophotometer. Measurements were made every cm for the upper 10.5 m of the core and below that this was done at 2 cm intervals.

## Results

### Age model

All the  $^{14}\text{C}$  samples were recalibrated following the approach outlined in De Deckker *et al.* (2020) for the adjacent core MD03-2611. Basically, marine radiocarbon reservoir ages (R) could be established based on the investigations of Sikes and Guilderson (2016), who were able to compare radiocarbon dates of planktic foraminifera from a core taken offshore the North Island of New Zealand and dated volcanic tephra layers that themselves were constrained by radiocarbon dates on land. Sikes and Guilderson (2016) conclude that R for subtropical waters was *ca* 700 years at *ca* 25 ka BP, *ca* 700–600 years for the

early deglaciation (*ca* 18–14 ka BP), and similar to today's value of *ca* 440 years for the Holocene. We follow the same approach taken by De Deckker *et al.* (2020) using an R of 700 years for samples older than 25 ka. In addition, for the older portion of the core, correlation is made with the Lisiecki and Stern (2016) regional benthic  $\delta^{18}\text{O}$  stack for the last glacial cycle. The benthic  $\delta^{18}\text{O}$  record of core MD97-2120 (45.53°S, 174.93°E; 1210 m; Pahnke & Zahn, 2005), selected by Lisiecki and Stern (2016), was chosen here for comparison with our core as the site for core MD03-2607 is bathed by intermediate waters similar to those from the Pacific Ocean (Supplemental material, Figure S4 shows the revised tie points with the Lisiecki and Stern [2016] curve). Based on the planktic  $\delta^{18}\text{O}$  record, the 125 ka BP age for the MIS 5e is easily identifiable as shown in Figure S4. Thus, the chronology of MD03-2607 is based on 24 calibrated radiocarbon and 19 OSL ages, plus some nine well-defined tie points on the Lisiecki and Stern [2016] curve. This core therefore is the best dated marine sequence in the Australian region spanning 125 ka on which 120 levels were examined for their palynological content, with on average one sample every 1000 years covering the last glacial/interglacial cycle.

The age-depth model for MD03-2607 shown in Supplemental material (Figure S4) was constructed using a Bayesian OxCal P sequence with variable deposition rate (*k*) and 'General' outlier analysis (prior probability = 0.05) (Bronk Ramsey, 2008, 2009; Bronk Ramsey & Lee, 2013). All the  $^{14}\text{C}$  results (except 2 possible problematic dates at 175 cm) and OSL dates (except 2 dates at 63.5 cm and 174.5 cm), as well as all the  $\delta^{18}\text{O}$  tie points are shown in Supplemental material (Figure S3; Table S1). The  $^{14}\text{C}$  dates used for the age-depth model are corrected for R values listed above and the SHCal20 curve (Hogg *et al.*, 2020) was used for age calibration.

### Pollen, spores and charcoal from MD03-2607

A percentage diagram of the pollen, spores and charcoal, as well as non-marine algae *Botryococcus*, *Debarya*, *Spirogyra* and *Zygnema*, counted in the 120 samples extracted from MD03-2607 is presented in Figure 3. Up to 50 taxa were identified, mostly at genus level, in addition to pteridophyte spores. Micro-charcoal particles were also counted on the pollen sample slides. The most common pollen taxa found in the core are: (listed in decreasing order of importance) Asteraceae–Tubuliflorae, Amaranthaceae–Chenopodiaceae, Poaceae, *Eucalyptus*, *Callitris*, *Casuarina*, *Melaleuca* and *Gyrostemon*. All the other taxa are in very low numbers when found, with the rare occurrence of *Nothofagus* likely derived from long-distance airborne dispersal. Concerning the Asteraceae, it was not possible to differentiate with confidence between various taxa in the samples from this core because of the large variety of Asteraceae types and variable state of preservation of the Asteraceae pollen grains that were present.

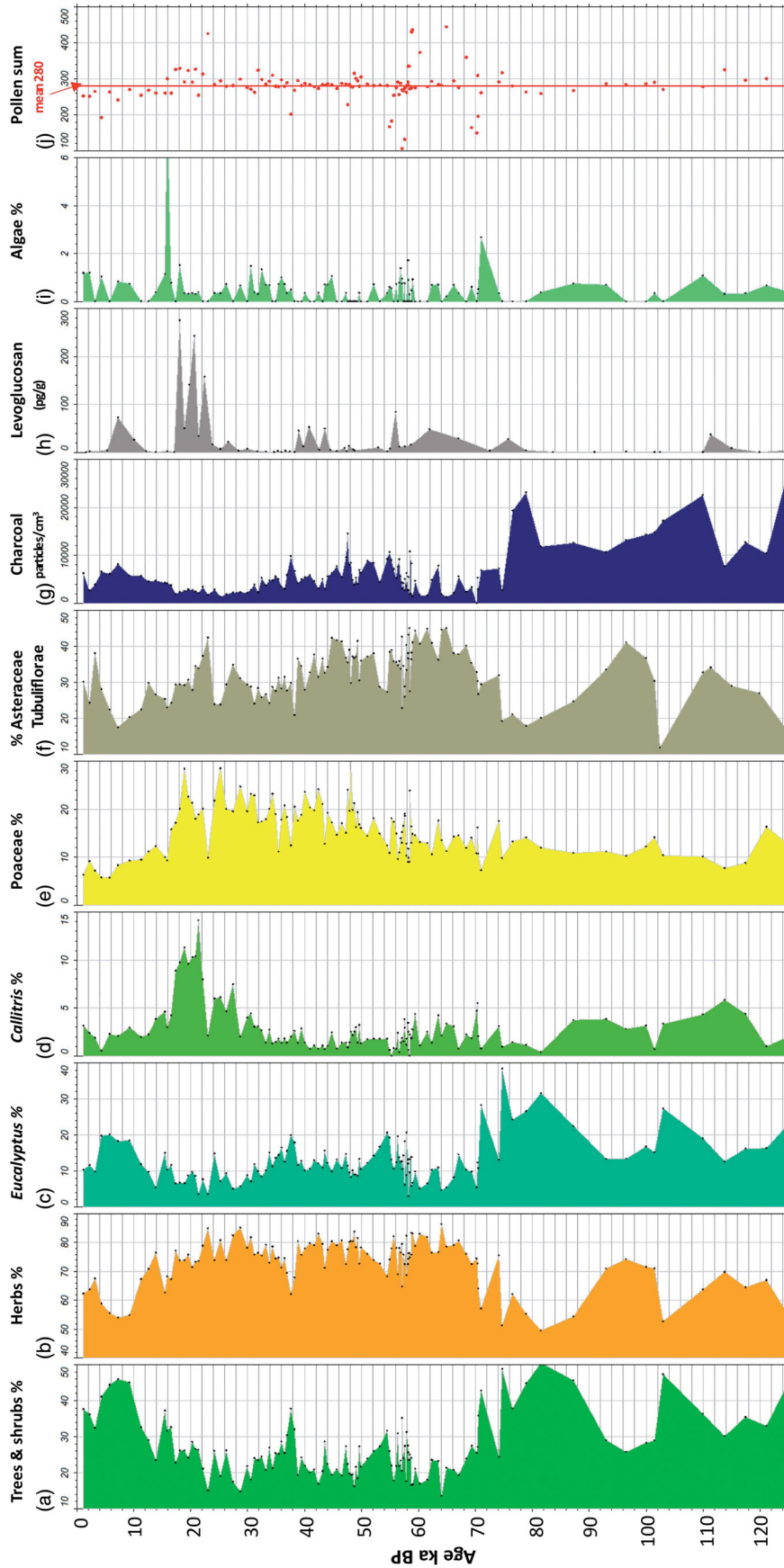


Figure 4. Diagram displaying percentages of selected important floral taxa, concentrations and the biomass-burning marker Levoglucosan determined from MD03-2607. (a) Combined tree and shrubs; (b) combined herbs; (c) *Eucalyptus*; (d) *Callitris*; (e) Poaceae; (f) Asteraceae/Tubuliflorae; (g) charcoal particle concentrations (particles/cm<sup>3</sup>); (h) Levoglucosan counts (per unit sediment mass) from Lopes dos Santos, De Deckker, Hopmans, et al. (2013); (i) algae; and (j) sum of pollen counted for each sample with values departing from the mean of 280 ± 48.

Note that some parts of the core had more levels examined for several reasons: (1) we targeted the period of time that approximately coincided with the published records of megafauna extinction; (2) emphasis was also placed on the period surrounding the LGM, and in particular, the maximum itself, but also the onset of deglaciation to determine the response of the vegetation to temperature rise, as well as the period that led to that of maximum cooling; and (3) MIS 4 had been targeted earlier by the detailed study of this 'penultimate glaciation' that can now be compared with MIS 2 and the cool interstadials such as MIS 5b and MIS 5d.

### **Palynological record from MD03-2607**

Marine isotopic stages have been placed on the pollen diagram (Figure 5) in order to see some of the salient patterns that coincide with warm (MIS 5e, 5c, 5a, 3 and 1 also referred to as the Holocene) and cold (MIS 5d, 5b, 4, 2 including the LGM) phases.

Before examining each stage separately, it is necessary to point out that two important tree taxa alternate over the last 125 ka: *viz.* *Eucalyptus* and *Callitris* percentages. *Callitris* is a long-lived gymnosperm that is fire-sensitive and found in undulating or flat land with sandy soils, or in upland rocky areas that are protected from fire. *Callitris* trees can also be present in *Acacia*, *Casuarina* and eucalypt forests with a shrubby, grassy or herb-rich understorey.

*Callitris* spp. display the highest percentages during the LGM and overall, also throughout the generally cold and dry MIS 2. Considerably higher values are also recorded during MIS 5d and 5c. In contrast, *Eucalyptus* spp. percentages are high during MIS 5e, the beginning of 5c, almost the entirety of 5a (when percentages are the highest), moderate during MIS 3 and high again during a large part of the Holocene. Of importance to note is that charcoal levels are highest when *Eucalyptus* spp. percentages are high.

The section below examines the distribution of the major taxonomic groups beginning from the base of the core for each marine isotopic stage shown in Figure 5.

#### **MIS 5 (1350 to 914 cm; 125 to 71 ka BP)**

This isotopic stage is divided into five phases, MIS 5e being the warmest and comprises the last interglacial sea-level high.

##### **MIS 5e (1350 to 1296 cm; 125 to 117 ka BP)**

*Eucalyptus* is the dominant tree taxon (Figure 4c) and charcoal levels are the highest at the same time (Figure 4g). Pteridophyte percentages are high (Figure 5f) as are those of *Gyrostemon* (Figure 5b). Grasses (Figure 4e) are present but in lower numbers than in younger parts of the core; Asteraceae/Tubuliflorae are present in substantial numbers (Figure 4f).

##### **MIS 5d (1296 to 1223 cm; 117 to 103 ka BP)**

At the beginning of this period, *Callitris* is the dominant tree taxon (Figure 4d) and this coincides with higher percentage of grasses (Figure 4b). *Gyrostemon* percentages (Figure 5b) drop down to very low levels in the middle of this stage. Pteridophyte counts are generally low but increase with time (Figure 5f). Charcoal levels are high for the second part of this stage (Figure 4g) and herb counts are high in the early part of this stage (Figure 4b).

##### **MIS 5c (1223 to 1085 cm; 103 to 92 ka BP)**

*Eucalyptus* values increase to the detriment of *Callitris* values (Figure 4c, d) and *Gyrostemon* and pteridophyte values increase (Figure 5b, f). Surprisingly, total percentage values for herbs are largely because of high numbers of Poaceae (Figure 4e) with Asteraceae almost non-existent (Figure 4f). Charcoal counts are also high (Figure 4g).

##### **MIS 5b (1085 to 1044 cm; 92 to 84 ka BP)**

The reverse abundance between *Callitris* and *Eucalyptus* occurs (Figure 4c, d), with the former having high numbers during this warm phase. Total herb counts increase compared with the previous stage (Figure 4b) and, although charcoal levels drop, they remain high (Figure 4g). Pteridophyte spores are absent (Figure 5f). *Gyrostemon* values are low overall (Figure 5b) and *Casuarina* percentages are moderately low during this period (Figure 5d). *Melaleuca* and myrtaceous shrubs (Figure 5e) returned their highest values, although still low with previous representation of these taxa (Myrtaceae and *Casuarina*).

##### **MIS 5a (1044 to 914 cm; 84 to 71 ka BP)**

*Eucalyptus* reaches maximum representation for the entirety of the core (Figure 4c) and charcoal levels are high (Figure 4g). *Callitris* values are at their lowest for MIS 5, except for one level in MIS 5e (Figure 4d). Pteridophyte numbers are higher, driven by high Cyatheaceae counts for the level at 72 ka BP (Figure 5f). Interestingly, Poaceae numbers still remain around 10% (Figure 4e) with *Gyrostemon* representation moderately high (Figure 5b).

##### **MIS 4 (914 to 818 cm; 71 to 59 ka BP)**

The vegetation spectra for this stage have already been examined in detail in De Deckker, Arnold, *et al.* (2019). Results are reiterated here: *Eucalyptus* and *Callitris* percentages are moderately low (Figure 4c, d) and herb percentages, particularly Poaceae, are high (Figure 4b, e). Charcoal counts are at their lowest (Figure 4g), with few pteridophyte spores encountered. *Gyrostemon* representation rises almost to the levels encountered during MIS 5d (Figure 5b). *Melaleuca* and myrtaceous shrub representation (although low overall, see Figure 5e) is the lowest for the entire sequence. Of particular interest is that during this

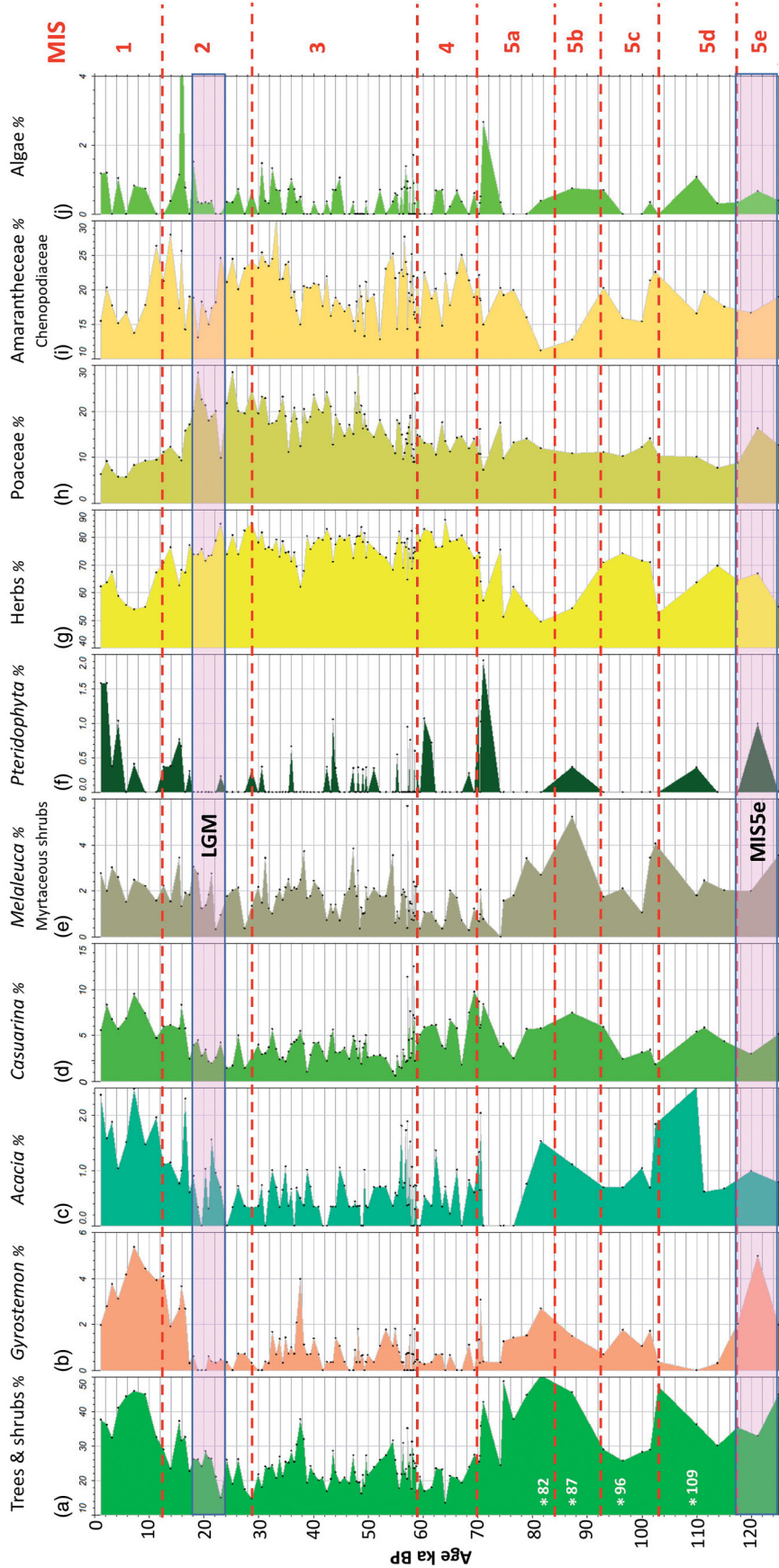


Figure 5. Diagram displaying percentages of selected taxa from MD03-2607 on which the various Marine Isotope Stages (MIS) are indicated, including the Last Glacial Maximum (LGM: 24–18 ka BP). (a) Combined trees and shrubs; (b) *Gyrostemon* sp.; (c) *Acacia*; (d) *Casuarina*; (e) *Melaleuca* and myrtaceous shrubs; (f) Pteridophyta; (g) total herbs; (h) Poaceae; (i) Amaranthaceae and Chenopodiaceae; and (j) algae. Compare the position of the Marine Isotope Stages with the zonation in Figure 3.

phase, *Casuarina* values are moderate (Figure 5d) and this may be related to the hydrological conditions.

### **MIS 3 (818 to 383 cm; 59 to 29 ka BP)**

This is a long-lasting stage (*ca* 30 ka BP) that eventually leads towards MIS 2 and the LGM. At the beginning of the stage, *Eucalyptus* percentages are higher than those of *Callitris*, but this changes before MIS 2 (Figure 4c, d). This switch is matched by a progressive increase in herbs percentages (Figure 4e), particularly after *ca* 47 ka BP when Poaceae increases after a minor spike in charcoal counts. Overall, charcoal counts remain low (Figure 4g) compared with the entirety of MIS 5. Pteridophyte counts remain low (Figure 5f) as well as those of *Gyrostemon* (Figure 5b) that are nevertheless slightly higher than for MIS 4.

### **MIS 2 (383 to 113 cm; 29–12 ka BP) and the LGM (316 to 194 cm; 24–18 ka BP)**

As observed in MIS 4, *Eucalyptus* values are low and *Callitris* numbers reach their highest level between 22 and 18 ka BP (Figure 4c, d). This is when Poaceae numbers are high (Figure 4e), *Gyrostemon* numbers low (Figure 5b) and charcoal levels at their lowest levels (Figure 4g) despite the fact that the coastline was very close (*~*15 km, see Figure 2) to the core site. After 18 ka BP, climate warms very rapidly (see De Deckker *et al.*, 2020, and discussion below) and, as a consequence, the pollen spectra change accordingly: the representation of *Callitris* drops (Figure 4d), as well as herbs (Figure 5g), pteridophyte number increase (Figure 5f) as does *Gyrostemon* (Figure 5b). *Melaleuca* and myrtaceous shrubs numbers (Figure 5e) are low, especially around 22 ka BP.

### **MIS 1 the Holocene (113 to top of core, 12 to *ca* 1 ka BP)**

*Eucalyptus* becomes the dominant dryland taxon (Figure 4c), with an increase in pteridophyte and *Gyrostemon* (Figure 5b, f) and herbs decrease (Figure 4b). Moderate *Casuarina* levels are a distinctive feature of this period (Figure 5d). Charcoal levels are a little higher (Figure 4g) but still not at the levels recorded in the lower parts of the core. Poaceae progressively decrease with time (Figure 4e).

We note that several minor taxa such as *Ficus* and Araucariaceae appear sporadically in the record of MD03-2607, but their percentages are too low to warrant any discussion on possible ecological/climatic implications. The same applies for *Phyllocladus* pollen, even slightly more common, but that are still in low numbers. Both *Phyllocladus* and Araucariaceae taxa appear during the warm phases, whereas *Ficus* is only present during MIS 5. We are aware that some of these taxa are found today in the tropics and subtropics of eastern Australia as well as the Victorian Otways and western Tasmania. It is possible therefore that pollen were transported to the core site via

oceanic currents, such as the East Australia Current poleward along the east coast of Australia, and the Flinders Current along the west coast of Tasmania that eventually passed over the core site (below the sea surface) on the way to the Great Australian Bight. Whether this means that those currents were stronger during the warm phases is a question that remains unanswered.

## **Discussion**

### **Algal record from MD03-2607**

The presence of four groups of non-marine algae, *Botryococcus*, *Debarya*, *Spirogyra* and *Zygnema*, throughout the core indicates, with some certainty, that the delivery of pollen, spores and charcoal to the core site must have been principally waterborne. To date, there has not been any record of *Botryococcus* cells found in airborne dust samples. This is supported by two examples of the palynoflora determined in airborne dust by S. van der Kaars in De Deckker *et al.* (2008), De Deckker *et al.* (2014), plus the study of pollen rain at Lake Frome by Singh (1981) and Lake George (Singh & Geissler, 1985) despite the fact that *Botryococcus* was recorded in the lake when water was present (De Deckker, pers. observ.).

In the next section, we present our determination of the source areas of fluvially transported sediments and associated pollen, spores and charcoal before examining the vegetation spectral changes for the entire MDB. Our assessment is based on the geochemistry of the sediments recovered from MD03-2607.

### **Charcoal and levoglucosan record of MD03-2607**

Figure 4g shows the record of charcoal counts in MD03-2607. The striking feature is that charcoal levels are continuously higher during the entirety of MIS 5. This coincides with the dominance of *Eucalyptus* pollen among the tree taxa. The other warm phase, MIS 1 (the Holocene) that also has high *Eucalyptus* percentages (Figure 4c), somewhat lower charcoal counts are recorded (Figure 4g). This difference may relate to a greater biomass of woody taxa available to burn during MIS 5 than during MIS 1, possibly a consequence of indigenous burning practices creating more open environments during the MIS 3 through to MIS 1.

An interesting aspect is that the high levoglucosan levels recorded from the same core by Lopes dos Santos, De Deckker, Hopmans, *et al.* (2013) do not coincide with the highest charcoal counts (Figure 4g, h). Levoglucosan is a specific organic compound resulting from the burning of cellulose at temperatures  $>300^{\circ}\text{C}$  (Simoneit, 2002), and it occurs in wood smoke plumes resulting from major fires that normally engender source-specific molecular traces such as levoglucosan (Simoneit *et al.*, 1999). It is therefore considered to be an indicator of biomass burning that can

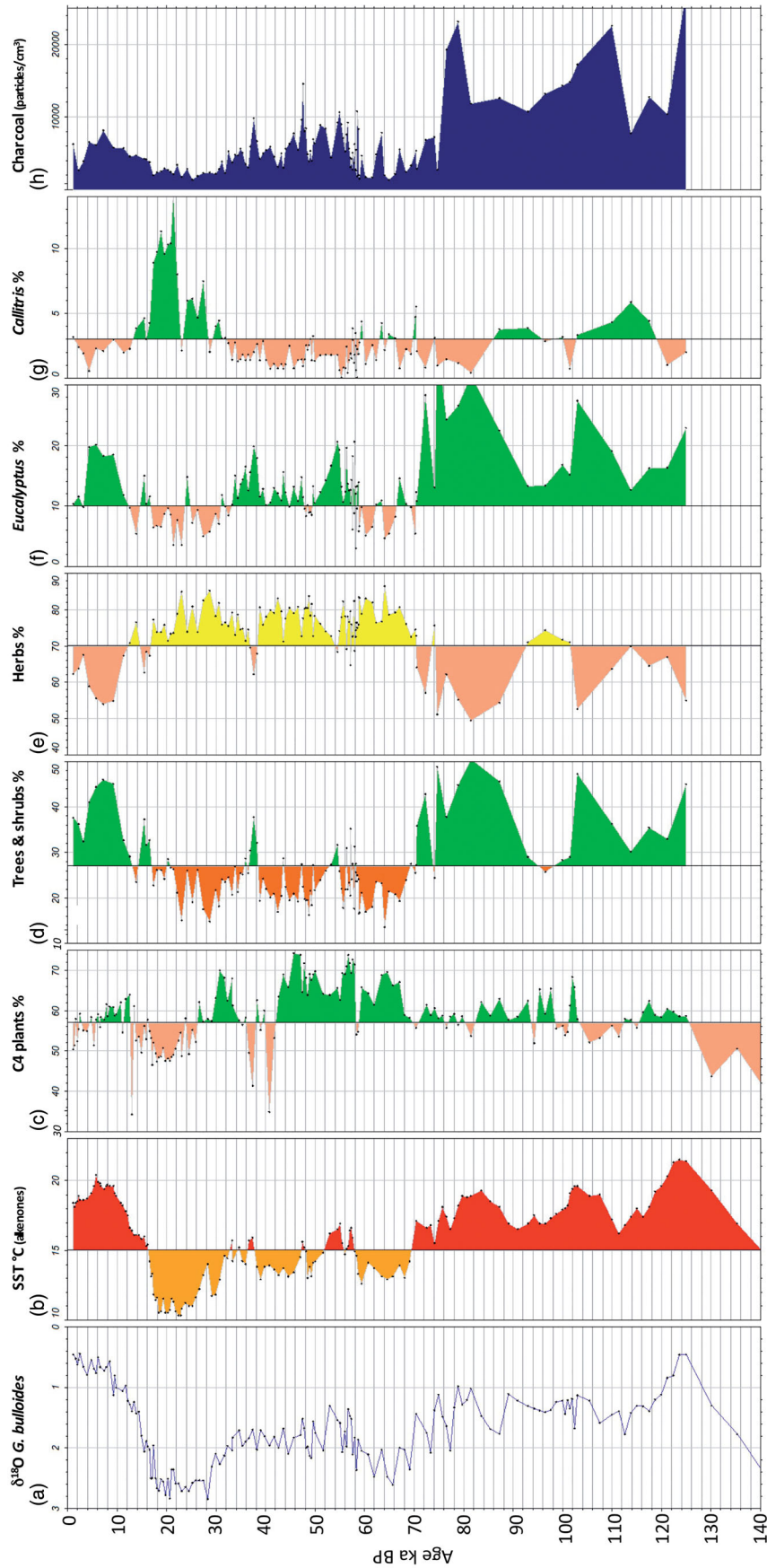


Figure 6. Plot of selected proxies obtained from MD03-2607. (a)  $\delta^{18}\text{O}$  of planktic foraminifera (proxy for sea-level change); (b) sea-surface temperatures (SST) based on alkenones (from Lopes dos Santos, Spooner *et al.*, 2013 and De Deckker, Arnold, *et al.*, 2019, combined); (c) percentage of C<sub>4</sub> plants (from Lopes dos Santos, De Deckker, P., Hopmans, *et al.*, 2013); (d) percentage of trees and shrubs combined; (e) all herbs combined; (f) *Eucalyptus* spp.; (g) *Callitris* sp.; and (h) concentrations (particles/cm<sup>3</sup>). The vertical arbitrary lines were placed on most plots to help visualise the shifts in percentages. The pink rectangles define the LGM. Marine Isotope Stages 4 and 5e.

travel long distances (Simoneit *et al.*, 1999). This may explain the lack of correspondence between levoglucosan peaks and high charcoal counts; levoglucosan is transported as an aerosol, whereas the charcoal recorded in the cores was mostly waterborne.

Broad patterns of levoglucosan counts (implying widespread biomass burning) show highest levels during the LGM at a time when SST were at their lowest (Figure 4h) and temperatures were also very low inland (Miller *et al.*, 1997). Levels also dropped during MIS 4 when SST were also very low. This may broadly represent a greater delivery of smoke particles to the coring site due to closer proximity of the exposed continent and smoke plumes blown seaward during elevated levoglucosan events, although the role of indigenous burning practices in this record should also be considered. Interestingly, during the LGM, biomass burning occurred when *Callitris* numbers were high (Figure 4d) but during the Holocene, when *Eucalyptus* was high, *Callitris* was low (Figure 4c, d). There is also a peak of levoglucosan in the middle of the Holocene when SST were at their highest. This is in contrast with MIS 5e, also characterised with the highest SST (Figure 6b), but levoglucosan levels were moderately low (Figure 4h). Levoglucosan levels were also moderately high with three peaks around 43 and 39 ka BP—with a revised chronology slightly differing from that of Lopes dos Santos, De Deckker, Hopmans, *et al.* (2013)—(Figure 4h) at a time when SST were low and the C<sub>3</sub>/C<sub>4</sub> plant ratio was low like during the LGM. Levoglucosan levels were very low during most of MIS 5c (warm phase) and MIS 5b (cool phase) (Figure 4h).

We note that our findings with high charcoal counts in MD03-2607 during the warm and wet phases match very well the observations made by Mooney *et al.* (2011). Based on 223 sedimentary charcoal records from Australasia, these authors determined (within limits of dating uncertainties of individual records) that, for the period spanning 73.5 to 14.7 ka BP for, the charcoal composite record shows substantial increases during Greenland Interstadials. This argues therefore for increases in biomass burning during those periods. Our charcoal counts record in MD03-2607 extends those findings further back in time.

### Comparison between selected taxa and the organic geochemical record (C<sub>3</sub>/C<sub>4</sub> plants)

Lopes dos Santos, De Deckker, Hopmans, *et al.* (2013) estimated the C<sub>3</sub>/C<sub>4</sub> plants ratios recorded in MD03-2607 based on the  $\delta^{13}\text{C}$  of *n*-alkanes of high plant wax *n*-alkanes. Several broad trends are seen: (1) during the glacial periods (MIS 2 and in particular the LGM, and MIS 6), there is a clear shift towards C<sub>3</sub> plants (<50% as shown in Lopes dos Santos, De Deckker, Hopmans, *et al.* (2013, figure 2f) for MIS 6 and ~50% for MIS 2); (2) concerning the period between 50 and 40 ka BP, there is a noticeable shift from C<sub>4</sub> to C<sub>3</sub> plants, that started just before 44 ka BP and

culminated 2000 years later (Figure 6c) (revised chronology from Lopes dos Santos, De Deckker, Hopmans, *et al.* (2013) due to the recalibration of the  $^{14}\text{C}$  dates with a new marine reservoir age). This coincides with moderate levels of levoglucosan for two millenia from ca 43 ka BP (Figure 4h), and it also coincided with a drop in SST of >2 °C that in fact had commenced much earlier (Figure 6b). This C<sub>3</sub>/C<sub>4</sub> shift in fact was maintained until ca 38 ka BP. Lopes dos Santos, De Deckker, Hopmans, *et al.* (2013) already discussed the possibility of biomass burning, following on from the megafauna extinction as the cause of vegetational changes. To add to this debate, Miller *et al.* (2005) reconstructed the paleodiets of the emu *Dromaius novaehollandiae* based on the  $\delta^{13}\text{C}$  of their eggshells and concluded that between 50 and 45 ka BP, the mean dietary  $\delta^{13}\text{C}$  of *D. novaehollandiae* decreased significantly. Before 50 ka BP, the emu diet was broad, as it ate a wide variety of food (both C<sub>3</sub> and C<sub>4</sub> plants), but after 45 ka BP, its food source changed to a dominance of C<sub>3</sub> plants. This dramatic shift is not noticeable in Lopes dos Santos, De Deckker, Hopmans, *et al.* (2013)'s record (Figure 6) as the latter covered analyses of all plant waxes, mostly from trees.

### Comparison of the palynofloral record with SST, oceanic conditions and the rainfall/moisture record from inland Australia

Lopes dos Santos, Spooner *et al.* (2013) compared various SST records for MD03-2607 based on several proxies (U<sup>K</sup><sub>37</sub> based on alkenones, TEX<sup>H</sup><sub>86</sub> based on glycerol dialkyl glycerol tetraethers [GDGTs], and LDI based on long-chain diols, in addition to foraminiferal faunal transfer function assemblages) but the latter three proxies are not discussed here. Instead, we only refer to the study of Lopes dos Santos, Spooner *et al.* (2013) and De Deckker, Arnold, *et al.* (2019) for the detailed record of SST reconstructions based on alkenometry (U<sup>K</sup><sub>37</sub>) for comparison with the palynoflora record (Figure 6b). This record ought to be considered as representative of temperature changes that must have occurred inland, especially since Miller *et al.* (1997) had already determined the temperature-dependent amino acid racemisation reaction rate from numerous dated fossil emu egg-shell fragments from the interior of Australia and estimated that average air temperatures were at least 9 °C lower than today for the 45 to 16 ka BP period. Such low temperatures had years before been postulated by Galloway (1965) who argued that during the glacial period in eastern Australia temperatures were at least 9 °C lower than today for the warmest month based on observations of solifluction slopes in the Australian Alps. Hence, it should be considered that the SST reconstructions could be applied to land temperature changes, not necessarily using similar values, but at least broad trends.

As presented earlier, *Callitris* percentages outweigh *Eucalyptus* percentages during the coldest phases, *viz.* MIS 2 and also MIS 5b and 5d (see Figure 6f, g). It is during the

LGM that *Callitris* reach highest numbers. During MIS 4, however, *Callitris* values are almost on par with *Eucalyptus* values and we postulate that this results from the upper part of the MDB, viz. the Darling sub-basin, being quite wet. Our reasoning for this is as follows: Miller, Fogel, et al. (2016) had examined the  $\delta^{18}\text{O}$  composition of the carbonate fraction from a vast amount of emu eggshells from five regions of Australia. They used the  $\delta^{18}\text{O}$  as a proxy for point potential evapotranspiration [PPET] for February–March (summer months). Only four are of interest to our study here: (1) sites around Kati Thanda-Lake Eyre in South Australia, (2) sites around Lakes Frome, Callabonna, Blanche and Gregory, South Australia, (3) sites in lake-shore lunettes along the lower Darling River, the Willandra Lakes and Lake Victoria, western New South Wales, and (4) sites between Port Augusta and Lake Torrens in South Australia. For all four regions, the PPET clearly indicated very wet conditions during MIS 4. We interpret from those findings that the upper part of the MDB, viz. the Darling sub-basin, must have been very wet during that period and may explain why *Callitris* values are not particularly high during the very cold MIS 4 period (also see De Deckker, Arnold, et al., 2019).

#### **Ordination plots to decipher affinities of selected samples with modern pollen sites**

Ordination was performed on percentage data from 15 of the most common pollen taxa in the Southeastern Australian Pollen Database (SEAPD) (D'Costa & Kershaw, 1995 for selected levels in MD03-2607 in R (R Core Team, 2020), widely chosen at the boundary of palynofloral changes using the non-metric multidimensional scaling routine within the vegan package (Oksanen et al., 2019). These samples are shown in Figure 7a with NMDS1 and 2 being the x and y axis of the dissimilarity matrix resulting from the ordination. Individual samples in Figure 7a show their respective ages that are compared against sites listed in the SEAPD. Figure 7b shows the modern-day rainfall isohyets for SE Australia pasted on the location of the sites from which pre-European pollen data are available. The approximate rainfall isohyets for 1993 were taken from the Atlas of Australian Resources (1993) and were chosen because they precede the significantly registered climatic changes in the region that have been considered to result from global warming.

It is important to note that those plots only provide information on today's rainfall levels projected for the past but should not be interpreted as being necessarily equivalent to past conditions at those sites. Note that there is quite a variation in similarity with today's pollen sites, even for the two samples that span the LGM, as shown by the brown triangles in Figure 7a.

#### **Comparison of the MD03-2607 pollen record with all other deep-sea cores from the Australian region**

Description of these cores and a discussion is provided in the Supplemental material. We note, however, that our study presented here is the only one of its kind for the Australian region, and perhaps for anywhere in the world, where numerous proxies (marine as well as non-marine) are compared against a pollen and algal record spanning the entire last glacial/interglacial record.

#### **Origin of the clays and clay fraction of the sediments in MD03-2607**

Before examining the origin of pollen, algae and charcoal recovered from MD03-2607, it is necessary to refer to the work of Gingele and De Deckker (2004, 2005b) on the clay fraction of sediments from rivers from the MDB. Basically, the MDB consists of two distinct geological entities: the northern tributaries of the Darling River originating from south-central Queensland where Mesozoic clastic sediments outcrop, and the eastern tributaries draining the western slopes of the Great Dividing Range, which consist of Cenozoic mafic volcanics, Mesozoic granites and late Paleozoic volcanics and metasediments; these form the southern part of the New England Fold Belt. The Murray and its tributaries drain the Lachlan Foldbelt that consist predominantly of Paleozoic granites, volcanics and metasediments. Gingele et al. (2004) and Gingele and De Deckker (2005b), who examined the clay composition and Sr and Nd isotope composition of river sediments in the MDB, clearly demonstrated that there is a strong link between the geology and the clays. The Darling sub-basin predominantly consists of smectite (Darling:  $31.4 \pm 25.3\%$ ; Murray:  $8.8 \pm 10.2$ ) with low  $^{87}\text{Sr}/^{86}\text{Sr}$  ratios and  $\epsilon\text{Nd}(0)$  values ranging from 1.4 to 6.7 ( $\epsilon\text{Nd}(0)$  = parts in 10 000 deviation from the terrestrial primitive mantle Nd isotopic composition). In contrast, the Murray sub-basin rivers are predominantly illite-rich (Darling:  $43.8 \pm 4.1\%$ ; Murray:  $27.1 \pm 14.9$ ) and have high  $^{87}\text{Sr}/^{86}\text{Sr}$  ratios and their  $\epsilon\text{Nd}(0)$  between  $-12$  and  $-9$ . Bayon et al. (2017) were also able to distinguish between the clay fraction of river sediments from within the MDB and came up with a clear distinction between fluvial sediments from the two sub-basins.

With such geochemical knowledge, Gingele and De Deckker (2005b) carried out a broad study of the two Murray Canyons Group cores MD03-2607 and MD03-2611 and determined a similar pattern for the clay composition in both cores. In MD03-2607, some 85 samples were analysed for the upper 1400 cm, whereas some 54 samples were examined for the entire MD03-2611 core. Gingele et al. (2007) used the same type of analyses (e.g. clay mineralogy as well as Sr and Nd isotopes) to examine in more detail the changes in sediment composition (and origin) of sediments in MD03-2611 spanning the last 17 ka. As a reliable chronology was not available at the time for the rest of the core, the distribution plot for MD03-2607 is now



are: (1) during a large part of MIS 5, the vegetation spectra must have originated from the Darling sub-basin, except for the ca 100 to 86 ka BP period that showed fluctuations between the two sub-basins; (2) the vegetation spectra during MIS 4 belonged to the Darling sub-basin; (3) during MIS 3, the Darling sub-basin was the main contributor of the palynoflora, except for an episode of Murray sub-basin influence during the ca 58–ca 49 ka BP period; (4) during MIS 2 and also in particular the LGM, a Darling sub-basin signature is clear; and (5) the Holocene has a very strong Murray sub-basin overprint, stronger than seen during MIS 5.

Since, Bayon *et al.*'s (2017) analyses did not extend below 1068 cm, we have to rely on Gingele and De Deckker (2005b) clay analyses, which show for a large portion of MIS 5, smectite % were rather low and therefore indicated a Murray sub-basin source (Figure 8b), except during MIS 5b and with no clear signal (or a mixed source) during MIS 5c.

When comparing the geochemical composition of the fluvial clays recovered from the core against the pollen record, obvious conclusions can be made concerning the potential origin of the palynoflora, knowing that it is more than likely to have been waterborne based on the presence of algae in all the samples (Figure 4i). Examination of Figure 8 shows that the shift in percentages between *Gyrostemon*, herbs and *Callitris* (Figure 8c–e), for example, shows clear shifts that parallel broad changes in the sediment composition. For example, during a large part of MIS 5, herbs (and assuming other pollen taxa) originated from the Darling sub-basin. *Gyrostemon*, on the other hand, displays an opposite trend (Figure 8c) coming from the Murray sub-basin. The data for MIS 3 and 2 show that the palynoflora originated from the Darling sub-basin and, because herb values are significantly high, whereas parts of the MDB would have been drier than the previous phase.

### Pollen dispersal and origin

There is only one study, by Mariani *et al.* (2016) in Tasmania in animal-pollinated vegetation mosaics, that modelled pollen dispersal in Australia. Two well-known pollen dispersal models were assessed the model performance and they found that pollen productivity estimates and relevant source area of pollen obtained using the Lagrangian Stochastic turbulent simulations appeared to be more realistic. Nevertheless, we could not use this approach as the pollen taxa in western Tasmania are very different from those of the MDB, and we could not rely on modern pollen distribution from that basin. Mariani *et al.* (2016) concluded that future work should consider both a test of pollen dispersal models combined with a choice of pollen productivity estimates which they postulated may result in substantial differences when estimating past vegetation cover. Much more work is needed in that domain.

However, we instead used a statistical program originally designed by sedimentologists to determine the origin of sediment particles in a basin (Dietze & Dietze, 2019). The

aim of this program is to decompose multi-modal grainsize distributions into inherent subpopulations, commonly termed 'End Member Modelling Analysis' that is used as a tool to infer the underlying sediment sources, transport and (post-)depositional processes. This End Member Modelling program using EMMAgeo (Dietze & Dietze, 2019, Dietze *et al.*, 2012) was undertaken in R (R Core Team, 2020) using our pollen data from MD03-2607. The pollen data were decomposed with the inversion algorithm for 'end-member modelling of compositional data' using EMMAgeo to construct a mixing model that expresses the observations as mixtures of a limited number of end members. Ultimately, four end members were obtained based on 16 selected taxa, and these listed extreme, theoretical pollen assemblages that are representative of different types of vegetation and potential source areas. More information is presented in the Supplemental material.

Statistical analysis placed proportions of the pollen percentage data into four distinct groups:

- **EM1:** An open *Eucalyptus* woodland with *Callitris* and *Casuarina* being the significant other woody components. Other woody elements such as *Acacia*, *Banksia*, *Dodonaea* and *Gyrostemon* are minor components within this vegetation type. The dominant woody herbaceous taxa are Asteraceae, Cyperaceae and Poaceae with a considerable amount of *Plantago*.
- **EM2:** An open mixed *Eucalyptus* forest with a considerable amount of *Acacia*, *Callitris*, *Casuarina* and *Gyrostemon*. The woody herbaceous component is largely comprised of Chenopodiaceae with much Asteraceae and Cyperaceae.
- **EM3:** An open woody herbaceous vegetation dominated by Asteraceae with a large number of Chenopodiaceae and, to a lesser degree, Poaceae. A limited number of woody taxa are present, principally *Casuarina* and *Eucalyptus*.
- **EM4:** An open grassland vegetation composed of Poaceae, Chenopodiaceae and Asteraceae with some Cyperaceae. *Callitris* and *Eucalyptus* are the tree taxa.

These groups are displayed in Figure 9 for the period 125 ka BP to the present. A shift in vegetation types through time is visible with clear changes at the MIS 5/4 boundary as well as after MIS 2. There is also a gradual decline in woody herbaceous vegetation during MIS 3 at the same time as an increase in woody grassland vegetation. Comparison of Figures 8 and 9 indicates that vegetation types identified as EM2 and EM3 occurred predominantly in the Darling sub-basin and EM1 and EM4 in the Murray sub-basin.

### Use of pollen transfer functions to reconstruction of mean annual rainfall

Estimates of mean annual rainfall generated from the pollen percentage data are presented in Figure 10b. Several

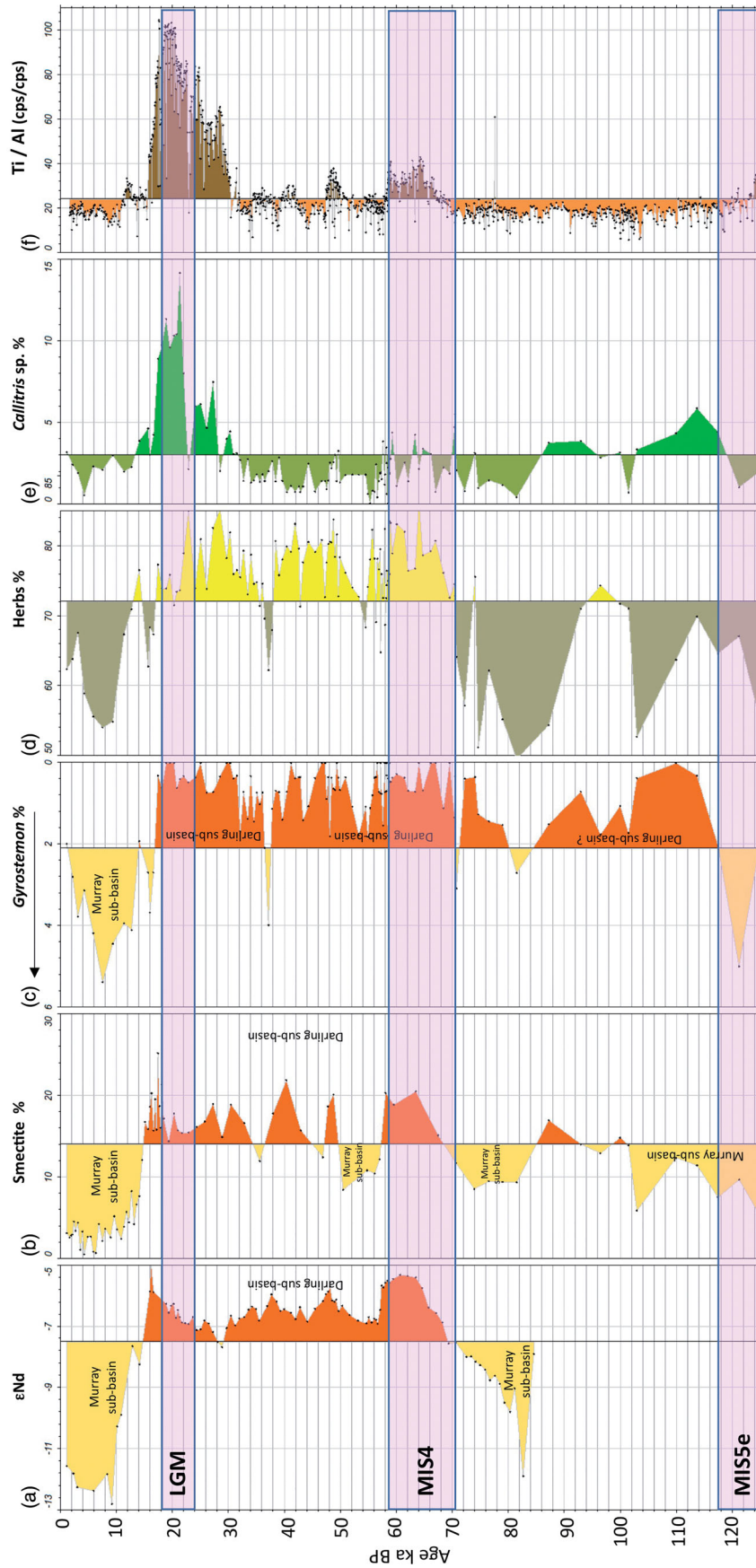
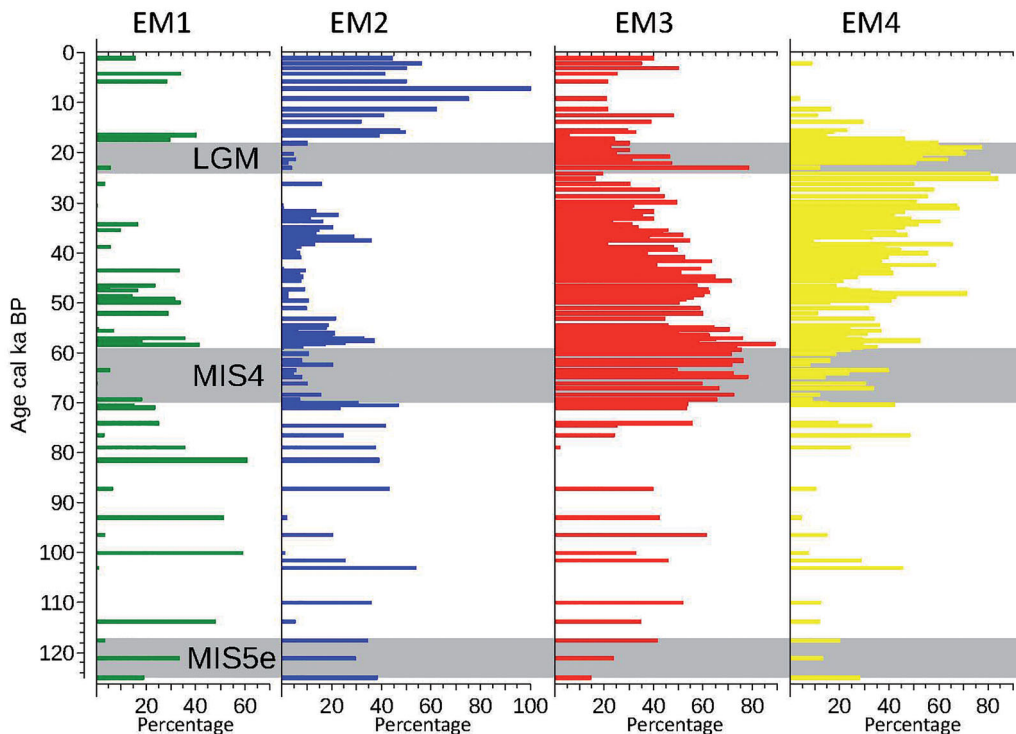


Figure 8. Plot of selected proxies obtained from MD03-2607. (a)  $\epsilon$ Nd isotopes from the clay fraction (from Gingele et al., 2004 on core MD03-2611 for the upper 16 ka of the record, and from Bayon et al. (2017) on core MD03-2607 for the rest of the record); (b) percentage of smectite clays (Gingele et al., 2007); (c) percentage of *Gyrostemon* pollen (the axis is reversed to help visualisation against other proxies); (d) percentages of total herbs; (e) *Callitris* pollen; and (f) Ti/Al (counts per second) obtained from XRF scanning. The pink rectangles cover the time spans for the LGM, MIS 4 and 5e. The vertical arbitrary lines were placed on all plots to help visualise the shifts in percentages. For the first three proxies, the beige shading relates to material originating from the Murray sub-basin in contrast with the orange shading that relates to the Darling sub-basin.



**Figure 9.** Plot of the four end members obtained by using the R package EMMAgeo for the all the pollen counts from MD03-2607. The plots are shown down core in calibrated ka BP and the horizontal axes give the percentages for each end-member. See text for more information.

salient features are noticeable: (1) there is good correspondence between SST changes and reconstructed rainfall, especially for the two predominantly 'glacial' phases, viz. MIS 4 and MIS 2. However, during MIS 3 SSTs remained low whereas rainfall was moderately high and more significantly than during a large part of MIS 5, and in particular MIS 5e to 5b, reconstructed rainfall was surprisingly low. This could result from the fact that there is no equivalent today in the region to climatic conditions that prevailed during a large part of MIS 5, including MIS 5e (Figure 10b), or that vegetation spectra were different for that period because humans had not interfered with the landscape compared with the Holocene. Of note also is that reconstructed rainfall for MIS 5a is as high as seen in the mid-Holocene.

#### **Link between *Eucalyptus* and fire activity shown by charcoal**

Fire in Australia is strongly related to the vegetation type, biomass and climate conditions that determine the susceptibility of vegetation to ignition (Bradstock, 2010; Russell-Smith *et al.*, 2007). The strong correspondence between charcoal concentration and *Eucalyptus* % likely reflects the significant role of flammable plant biomass in charcoal production that leads to the deposition of microcharcoal in MD03-2607 (Figure 10c, d). Unfortunately, Mooney *et al.* (2011), who examined the charcoal records from some 223 sites in Australasia, did not discuss the possible link between high charcoal counts and the type of vegetation.

In the case of MD03-2607, the decline in charcoal concentration appears to be primarily driven by a combination of declining biomass with the expansion of grasslands (drier conditions) and cooler climate limiting fire ignition (reduced probability of fire ignition). The addition of indigenous fire management into the Australian landscape, possibly between 65 and 40 ka BP (Clarkson *et al.*, 2017; O'Connell & Allen, 2015) is not clearly reflected in the charcoal record of MD03-2607. However, the brief spike in charcoal concentration and subsequent expansion of open environments may well be an ecosystem response to the shift to the widespread practice of frequent and low intensity fires across the MDB around 47–43 ka BP (Figures 5h and 10c). This pattern is in line with other terrestrial records interpreted to reflect human impact on fire regimes in Australia during MIS 3 such as Lynch's Crater in north-east Australia (Rule *et al.*, 2012) and the Cape Pasley marine core in southwest Australia (Cape Pasley marine core MD03-2614G; van der Kaars *et al.*, 2017).

#### **Comparison with pollen records obtained from inland Australia**

Luly (2001) examined the pollen record from a 3.7 m long core at Lake Frome in central South Australia (Figure 1) and showed that *Callitris* dominated woodlands were predominant in the vicinity of the large playa lakes, Frome and Eyre, during the late Pleistocene. He determined that *Callitris* woodlands were present at Lake Eyre before 30 ka BP (uncalibrated years) but became increasingly

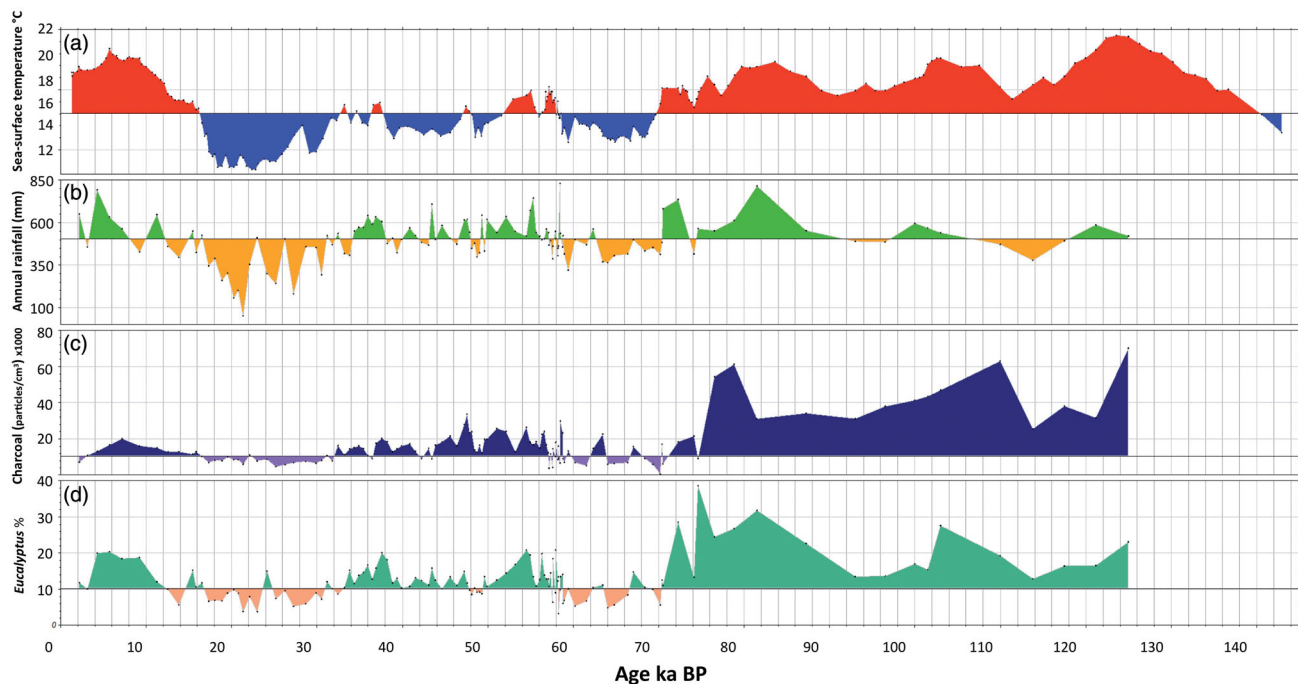


**Figure 10.** Comparative plots for four proxies obtained from MD03-2607 for the last 125 ka. (a) Sea-surface temperature (SST) obtained by alkenometry (combined data from Lopes dos Santos, Spooner *et al.* (2013) and De Deckker, Arnold, *et al.* (2019)); (b) reconstructed annual rainfall using the transfer function developed by Cook and van der Kaars (2006); (c) charcoal concentrations (particles/cm<sup>3</sup>) (note values are to be multiplied by 1000); and (d) percentages of *Eucalyptus* pollen. The horizontal arbitrary lines were placed to help visualise the shifts in values and for comparison between the plots. There appears to be good correspondence for most periods between rainfall and SST, and charcoal concentration and *Eucalyptus* percentages.

fragmented and eventually vanished in the lead up to the LGM. At Lake Frome, however, *Callitris* was 'abundant between 16 and 13 ka (uncalibrated years) before declining to the low levels (seen today) from 11 000 BP'. That study also mooted that the demise of *Callitris* woodlands was caused by Aboriginal fire practices. An alternative that we suggest is that a change in rainfall and rise of temperatures may have led to those vegetation changes. For example, *Callitris* is eventually replaced in the Lake Frome record initially by *Eucalyptus* after the LGM and then, during the mid-Holocene, by *Casuarina*, a pattern also exhibited in MD03-2607. We note that, in contrast with MD03-2607, charcoal counts are much higher in the Lake Frome record during the *Callitris* dominated phase, which may reflect a regional burning of mixed sclerophyll woodlands rather than direct burning of fire-sensitive *Callitris* woodlands.

More recently, Sniderman *et al.* (2019) studied the pollen record preserved in a speleothem from Mammoth Cave (34.06°S, 115.03°E) located in the Leeuwin-Naturaliste region of SW Western Australia. The record is dated using some 30U–Th dates and is characterised by the almost complete absence of *Eucalyptus* pollen during the entirety of MIS 2 (with a gap with no pollen recovered). In contrast with the pollen signal from MD03-2607, the predominant woody taxon was Casuarinaceae, occurring together with herb vegetation Poaceae and Asteraceae. *Callitris* was absent from the Mammoth Cave record, perhaps because the local soils were derived from the limestone regolith; *Callitris* tends to grow on sandy soils and in particular

quartz-rich sandy dunes; refer to Clayton-Greene (1981) and Ngugi *et al.* (2013) for more information on the variety of soils several *Callitris* species are found on. Both records from Mammoth Cave and MD03-2607 demonstrate that MIS 2 was much drier than the last part of MIS 3 and the Holocene.

The Supplemental material provides a detailed analysis of the pollen record obtained from all the marine cores taken in the Australian region. Some of the data recovered from these are compared with the pollen record of MD03-2607.

## Conclusions

The palynofloral and charcoal record of core MD03-2607 provides for the first time a detailed record of vegetation changes for a very large part of SE Australia, *viz.* the Murray-Darling Basin (MDB), which today in its northern portion (the Darling sub-basin) fringes the arid zone. We argue that most of the pollen was transported by water as all samples contain non-marine algae. Using geochemical markers from the clay fraction of fluvial sediments obtained from the same core, we identify the periods that the palynofloral spectra derive from the Murray sub-basin and the times they derive from the Darling sub-basin. There is also an airborne component in the core in the form of eolian dust as well as the aerosol levoglucosan, indicative of widespread biomass burning. We also surmise that it is possible that when the eolian dust was dominant, especially during

the LGM, grass pollen may also have originated from an unknown part of the MDB.

The overall palynoflora trends in MD03-2607 fit well with the  $C_3/C_4$  ratios reconstructed by Lopes dos Santos, De Deckker, Hopmans, *et al.* (2013) and match the preliminary findings by Gröcke (1997), who reconstructed general changes in  $C_3/C_4$  vegetation from the diet of megafauna from different sites in South Australia as determined by the  $\delta^{13}C$  composition of their collagen. Our detailed investigations on MD03-2607 endorse the extrapolation made by Miller *et al.* (2005) that there was no significant climate change around 45 ka BP; SSTs only dropped slightly at that time, broad vegetation patterns did not alter significantly, and charcoal counts were not necessarily higher.

The regional record of the MDB demonstrates the following:

1. *Callitris* alternated with *Eucalyptus* as the dominant dryland taxon, with the former reaching greatest numbers during MIS 2. This is a trend also noticeable in the GC17 record with *Callitris* more dominant during glacial conditions. The same was found in core E55-6 during MIS 2, but only one sample was analysed. Similarly, in core MD03-2614, offshore Western Australia, at the LGM *Callitris* values rose while *Eucalyptus* remained low although only one sample was analysed for that period. In ODP core 820A, there was little *Callitris* pollen recorded to make a comparison with *Eucalyptus* numbers.
2. High charcoal concentrations correlate with high *Eucalyptus* numbers, especially during the warm and wet periods. However, the presence of the biomass marker levoglucosan, studied by Lopes dos Santos, De Deckker, Hopmans, *et al.* (2013), does not coincide with high charcoal counts. This aerosol must have originated from an unknown source within the MDB and may partly reflect proximity of the coastline. This needs to be further investigated.
3. Comparison of the palynoflora with SSTs recorded offshore shows that when SSTs were high, *e.g.* during the entirety of MIS 5 and MIS 3 and part of the Holocene, *Eucalyptus* dominated the dryland vegetation.
4. Orbital-scale climate change is clearly imprinted on the pollen and charcoal record of MD03-2607. However, there is a suggestion that minor peaks in charcoal and levoglucosan concentration, as well as grassland expansion around 47–43 ka BP could be related to anthropogenic influence on fire regimes in the MDB as already pointed out by Lopes dos Santos, De Deckker, Hopmans, *et al.* (2013). This will be examined in a forthcoming paper that discusses the presence of fungal spores associated with the presence of megafauna.

## Acknowledgements

The core was obtained with the skilful help of Yvon Balut, the RV *Marion Dufresne* manager, during the AUSCAN cruise. The authors are

grateful to Professors Peter Kershaw and Mary-Anne Geurts for supplying *Lycopodium* tablets, no longer available on the market. Martine Hagen at the Sediment Laboratory of the Vrije Universiteit Amsterdam prepared the samples for pollen counting.

The authors acknowledge the very helpful comments from reviewer Peter Kershaw and additional comments from an anonymous reviewer.

## Disclosure statement

No potential conflict of interest was reported by the author(s).

## Funding

The AUSCAN cruise that was partly funded by a grant to PDD from the National Oceans Office and support from the French Polar Institute and Australian Research Council. The ARC Centre of Excellence CE170100015 contributed to some of the costs of pollen preparation and analysis, as well as for 3 AMS dates carried out at ANSTO.

## ORCID

P. De Deckker  <http://orcid.org/0000-0003-3003-5143>  
 S. van der Kaars  <http://orcid.org/0000-0002-2511-0439>  
 S. Haberle  <http://orcid.org/0000-0001-5802-6535>  
 Q. Hua  <http://orcid.org/0000-0003-0179-8539>  
 J.-B. W. Stuut  <http://orcid.org/0000-0002-5348-2512>

## Data availability statement

More details are available on the journal website at <https://doi.org/10.1080/08120099.2021.1896578> and the entire pollen data are stored at <https://doi.pangaea.de/10.1594/PANGAEA.928645>.

## References

- Atlas of Australian Resources (1993). *Third Series, Volume 4, Climate*. Division of National Mapping.
- Barrows, T. T., & Juggins, S. (2005). Sea-surface temperatures around the Australian margin and Indian Ocean during the Last Glacial Maximum. *Quaternary Science Reviews*, 24(7–9), 1017–1047. <https://doi.org/10.1016/j.quascirev.2004.07.020>
- Bayon, G., De Deckker, P., Magee, J. W., Germain, Y., Bermell, S., Tachikawa, K., & Norman, M. D. (2017). Extensive wet episodes in Late Glacial Australia resulting from high-latitude forcings. *Scientific Reports*, 7, 44054. <https://doi.org/10.1038/srep44054>
- Bradstock, R. A. (2010). A biogeographic model of fire regimes in Australia: current and future implications. *Global Ecology and Biogeography*, 19(2), 145–158. <https://doi.org/10.1111/j.1466-8238.2009.00512.x>
- Bronk Ramsey, C. (2008). Deposition models for chronological records. *Quaternary Science Reviews*, 27(1–2), 42–60. <https://doi.org/10.1016/j.quascirev.2007.01.019>
- Bronk Ramsey, C. (2009). Bayesian analysis of radiocarbon dates. *Radiocarbon*, 51(1), 337–360. <https://doi.org/10.1017/S0033822200033865>
- Bronk Ramsey, C., & Lee, S. (2013). Recent and planned developments of the program OxCal. *Radiocarbon*, 55(2), 720–730. <https://doi.org/10.1017/S0033822200057878>
- Clarkson, C., Jacobs, Z., Marwick, B., Fullagar, R., Wallis, L., Smith, M., Roberts, R. G., Hayes, E., Lowe, K., Carah, X., Florin, S. A., McNeil, J., Cox, D., Arnold, L. J., Hua, Q., Huntley, J., Brand, H. E. A., Manne, T.,

- Fairbairn, A., ... Pardoe, C. (2017). Human occupation of northern Australia by 65,000 years ago. *Nature*, 547(7663), 306–310. <https://doi.org/10.1038/nature22968>
- Clayton-Greene, K. A. (1981). *The autecology of Callitris collumellaris* F. Muell. and associated *Eucalyptus* spp. in south-eastern Australia [unpublished PhD thesis]. The University of Melbourne, p. 371.
- Cook, E. J., & van der Kaars, S. (2006). Development and testing of transfer functions for generating quantitative climatic estimates from Australian pollen data. *Journal of Quaternary Science*, 21(7), 723–733. <https://doi.org/10.1002/jqs.1076>
- D'Costa, D. M., & Kershaw, A. P. (1995). A Late Pleistocene and Holocene pollen record from Lake Terang, western plains of Victoria, Australia. *Palaeogeography, Palaeoclimatology, Palaeoecology*, 113(1), 57–67. [https://doi.org/10.1016/0031-0182\(95\)00062-Q](https://doi.org/10.1016/0031-0182(95)00062-Q)
- De Deckker, P., Abed, R. M. M., De Beer, D., Hinrichs, K., O'Loingsigh, T., Schefuß, E., Stuut, J. W., Tapper, N. J., & van Der Kaars, S. (2008). Geochemical and microbiological fingerprinting of airborne dust that fell in Canberra, Australia, in October 2002. *Geochemistry, Geophysics, Geosystems*, 9(12). <https://doi.org/10.1029/2008GC002091>
- De Deckker, P., Arnold, L. J., van der Kaars, S., Bayon, G., Stuut, J-B W., Perner, K., Lopes dos Santos, R., Uemura, R., & Demuro, M. (2019). Marine Isotope Stage 4 in Australasia: A full glacial culminating 65,000 years ago—global connections and implications for human dispersal. *Quaternary Science Reviews*, 204, 187–207. <https://doi.org/10.1016/j.quascirev.2018.11.017>
- De Deckker, P., Moros, M., Perner, K., Blanz, T., Wacker, L., Schneider, R., Barrows, T. T., O'Loingsigh, T., & Jansen, E. (2020). Climatic evolution in the Australian region over the last 94 ka—spanning human occupancy—and unveiling the Last Glacial Maximum. *Quaternary Science Reviews*, 249, 106593. <https://doi.org/10.1016/j.quascirev.2020.106593>
- De Deckker, P., Munday, C., Brocks, J., O'Loingsigh, T., Alison, G., Hope, J., Norman, M., Stuut, J.-B., Tapper, N. J., & van Der Kaars, S. (2014). Characterisation of the major dust storm that traversed over eastern Australia in September 2009; a multidisciplinary approach. *Aeolian Research*, 15, 133–149. <https://doi.org/10.1016/j.aeolia.2014.07.003>
- De Deckker, P., van der Kaars, S., Macphail, M., & Hope, G. (2019). Land-sea correlations in the Australian region: 460k years of changes recorded in a deep-sea core offshore Tasmania. Part 1: The pollen record. *Australian Journal of Earth Sciences*, 66(1), 1–15. <https://doi.org/10.1080/08120099.2018.1495100>
- Dietze, E., & Dietze, M. (2019). Grain-size distribution unmixing using the R package EMMAge. *E&G Quaternary Science Journal*, 68(1), 29–46. <https://doi.org/10.5194/egqsj-68-29-2019>
- Dietze, E., Hartmann, K., Diekmann, B., Ijmker, J., Lehmkuhl, F., Opitz, S., Stauch, G., Wünnemann, B., & Borchers, A. (2012). An end-member algorithm for deciphering modern detrital processes from lake sediments of Lake Donggi Cona, NE Tibetan Plateau, China. *Sedimentary Geology*, 234–244, 169–180. <https://doi.org/10.1016/j.sedgeo.2012.09.006>
- Dietze, M., Dietze, E. (2016). EMMAgeo: End-member modelling of grain-size data, available at: <https://cran.r-project.org/web/packages/EMMAgeo/>
- Galloway, R. W. (1965). Late Quaternary climates of Australia. *The Journal of Geology*, 73(4), 603–618. <https://doi.org/10.1086/627096>
- Gingele, F. X., & De Deckker, P. (2005a). Late Quaternary fluctuations of palaeoproductivity in the Murray Canyons area, South Australian continental margin. *Palaeogeography Palaeoclimatology Palaeoecology*, 220(3–4), 361–373. <https://doi.org/10.1016/j.palaeo.2005.01.012>
- Gingele, F. X., & De Deckker, P. (2005b). Clay mineral, geochemical and Sr–Nd-isotopic fingerprinting of sediments in the Murray–Darling fluvial system, SE Australia. *Australian Journal of Earth Sciences*, 52(6), 965–974. <https://doi.org/10.1080/08120090500302301>
- Gingele, F. X., De Deckker, P., & Hillenbrand, C.-D. (2004). Late Quaternary terrigenous sediments from the Murray Canyons area, offshore South Australia and their implications for sea level change, palaeoclimate and palaeodrainage of the Murray–Darling Basin. *Marine Geology*, 212(1–4), 183–197. <https://doi.org/10.1016/j.margeo.2004.09.001>
- Gingele, F. X., De Deckker, P., & Norman, M. (2007). Late Pleistocene and Holocene climate of SE Australia reconstructed from dust and river loads deposited offshore the River Murray Mouth. *Earth and Planetary Science Letters*, 255(3–4), 257–272. <https://doi.org/10.1016/j.epsl.2006.12.019>
- Grimm, E. C. (1987). CONISS: A Fortran 77 program for stratigraphically constrained cluster analysis by the method of incremental sum of squares. *Computers & Geosciences*, 13(1), 13–35. [https://doi.org/10.1016/0098-3004\(87\)90022-7](https://doi.org/10.1016/0098-3004(87)90022-7)
- Gröcke, D. R. (1997). Distribution of C3 and C4 plants in the Late Pleistocene of South Australia recorded by isotope biogeochemistry of collagen in megafauna. *Australian Journal of Botany*, 45(3), 607–617. <https://doi.org/10.1071/BT96040>
- Harle, K. J. (1997). Late Quaternary vegetation and climate change in southeastern Australia: Palynological evidence from marine core E55-6. *Palaeogeography, Palaeoclimatology, Palaeoecology*, 131(3–4), 465–483. [https://doi.org/10.1016/S0031-0182\(97\)00016-3](https://doi.org/10.1016/S0031-0182(97)00016-3)
- Hill, P., & De Deckker, P. (2004). AUSCAN Seafloor Mapping and Geological Sampling Survey on the Australian Southern Margin by RV Marion Dufresne in 2003. Geoscience Australia Record, 2004/04, 136 pp.
- Hill, P., De Deckker, P., von der Borch, C. C., & Murray-Wallace, C. V. (2009). The ancestral Murray River on the Lacedpede Shelf, southern Australia: Late Quaternary migrations of a major river outlet and strandline development. *Australian Journal of Earth Sciences*, 56(2), 135–157. <https://doi.org/10.1080/08120090802546993>
- Hill, P. J., de Deckker, P., & Exon, N. F. (2005). Geomorphology and evolution of the gigantic Murray canyons on the Australian southern margin. *Australian Journal of Earth Sciences*, 52(1), 117–136. <https://doi.org/10.1080/08120090500100085>
- Hogg, A. G., Heaton, T. J., Hua, Q., Palmer, J. G., Turney, C. S. M., Southon, J., Bayliss, A., Blackwell, P. G., Boswijk, G., Bronk Ramsey, C., Pearson, C., Petchey, F., Reimer, P., Ron Reimer, R., & Wacker, L. (2020). SHCal20 Southern Hemisphere calibration, 0–55,000 years cal BP. *Radiocarbon*, 62(4), 759–778. <https://doi.org/10.1017/RDC.2020.59>
- James, N. P., & Bone, Y. (2011). *Neritic Carbonate Sediments in a Temperate Realm*. Springer. p. 254. <https://doi.org/10.1007/978-90-481-9289-2>
- Juggins, S. (2013). Quantitative reconstructions in palaeolimnology: new paradigm or sick science? *Quaternary Science Reviews*, 64, 20–32. <https://doi.org/10.1016/j.quascirev.2012.12.014>
- Lambeck, K., Rouby, H., Purcell, A., Sun, Y., & Sambridge, M. (2014). Sea level and global ice volumes from the Last Glacial Maximum to the Holocene. *Proceedings of the National Academy of Sciences of the United States of America*, 111(43), 15296–15303. <https://doi.org/10.1073/pnas.1411762111>
- Lisiecki, L. E., & Raymo, M. E. (2005). A Pliocene–Pleistocene stack of 57 globally distributed benthic  $\delta^{18}\text{O}$  records. *Paleoceanography*, 20(1). <https://doi.org/10.1029/2004PA001071>
- Lisiecki, L. E., & Stern, J. V. (2016). Regional and global benthic  $\delta^{18}\text{O}$  stacks for the last glacial cycle. *Paleoceanography*, 31(10), 1368–1394. <https://doi.org/10.1002/2016PA003002>
- Lopes dos Santos, R. A., Wilkins, D., De Deckker, P., & Schouten, S. (2012). Late Quaternary productivity changes from offshore Southeastern Australia: A biomarker approach. *Palaeogeography, Palaeoclimatology, Palaeoecology*, 363–364, 48–56. <https://doi.org/10.1016/j.palaeo.2012.08.013>
- Lopes dos Santos, R., De Deckker, P., Hopmans, E. C., Magee, J. W., Mets, A., Sinninghe, J. S., & Schouten, S. (2013). Abrupt vegetation

- change after the Late Quaternary megafaunal extinction in south-eastern Australia. *Nature Geoscience*, 6(8), 627–631. <https://doi.org/10.1038/ngeo1856>
- Lopes dos Santos, R., De Deckker, P., Sinninghe, J. S., & Schouten, S. (2013). A late Quaternary sedimentary record of steryl alkyl ethers from offshore southeastern Australia. *Organic Geochemistry*, 54, 140–145. <https://doi.org/10.1016/j.orggeochem.2012.10.010>
- Lopes dos Santos, R., Spooner, M. I., Barrows, T. T., De Deckker, P., Sinninghe, J. S., & Schouten, S. (2013). Comparison of organic ( $U^{K_{37}}$ ,  $TEX^{H_{86}}$ , LDI) and faunal proxies (foraminiferal assemblages) for reconstruction of late Quaternary sea surface temperature variability from offshore southeastern Australia. *Paleoceanography*, 28(3), 377–311. <https://doi.org/10.1002/palo.20035>
- Lourens, L. J. (2004). Revised tuning of Ocean Drilling Program Site 964 and KC01B (Mediterranean) and implications for the  $\delta^{18}O$ , tephra, calcareous nannofossil, and geomagnetic reversal chronologies of the past 1.1 Myr. *Paleoceanography*, 19(3). <https://doi.org/10.1029/2003PA000997>
- Luly, J. (2001). On the equivocal fate of Late Pleistocene *Callitris* Vent. (Cupressaceae) woodlands in arid South Australia. *Quaternary International*, 83–85, 155–168. [https://doi.org/10.1016/S1040-6182\(01\)00037-4](https://doi.org/10.1016/S1040-6182(01)00037-4)
- Mariani, M., Connor, S. E., Theuerkauf, M., Kunes, P., & Fletcher, M-S. (2016). Testing quantitative pollen dispersal models in animal-pollinated vegetation mosaics: An example from temperate Tasmania. *Quaternary Science Reviews*, 154, 214–225. <https://doi.org/10.1016/j.quascirev.2016.10.020>
- Miller, G. H., Fogel, M. L., Magee, J. W., & Gagan, M. K. (2016). Disentangling the impacts of climate and human colonization on the flora and fauna of the Australian arid zone over the past 100 ka using stable isotopes in avian eggshell. *Quaternary Science Reviews*, 151, 27–57. <https://doi.org/10.1016/j.quascirev.2016.08.009>
- Miller, G. H., Fogel, M. L., Magee, J. W., Gagan, M. K., Clarke, S. J., & Johnson, B. J. (2005). Ecosystem collapse in Pleistocene Australia and a human role in megafaunal extinction. *Science (New York, N.Y.)*, 309(5732), 287–290. <https://doi.org/10.1126/science.1111288>
- Miller, G. H., Magee, J. W., & Jull, A. T. J. (1997). Low-latitude glacial cooling in the Southern Hemisphere from amino-acid racemization in emu eggshells. *Nature*, 385(6613), 241–244. <https://doi.org/10.1038/385241a0>
- Mooney, S. D., Harrison, S. P., Bartlein, P. J., Daniau, A-L., Stevenson, J., Brownlie, K. C., Buckman, S., Cupper, M., Luly, J., Black, M., Colhoun, E., D'Costa, D., Dodson, J., Haberle, S., Hope, G. S., Kershaw, P., Kenyon, C., McKenzie, M., & Williams, N. (2011). Late Quaternary fire regimes of Australasia. *Quaternary Science Reviews*, 30(1–2), 28–46. <https://doi.org/10.1016/j.quascirev.2010.10.010>
- Moss, P. T., & Kershaw, A. P. (2000). The last glacial cycle from the humid tropics of northeastern Australia: Comparison of a terrestrial and a marine record. *Palaeogeography Palaeoclimatology Palaeoecology*, 155(1–2), 155–176. [https://doi.org/10.1016/S0031-0182\(99\)00099-1](https://doi.org/10.1016/S0031-0182(99)00099-1)
- Ngugi, M. R., Botkin, D. B., Doley, D., Cant, M., & Kelley, J. (2013). Restoration and management of callitris forest ecosystems in Eastern Australia: Simulation of attributes of growth dynamics, growth increment and biomass accumulation. *Ecological Modelling*, 263, 152–161. <https://doi.org/10.1016/j.ecolmodel.2013.05.004>
- O'Connell, J. F., & Allen, J. (2015). The process, biotic impact, and global implications of the human colonization of Sahul about 47,000 years ago. *Journal of Archaeological Science*, 56, 73–84. <https://doi.org/10.1016/j.jas.2015.02.020>
- Oksanen, J., Guillaume Blanchet F., Friendly M., Kindt R., Legendre P., McGlenn D., Minchin P. R., O'Hara R. B., Simpson G. L., Solymos P., Stevens M. H. H., Szoecs E., Wagner H. (2019). *Vegan: Community Ecology Package*. R package version 2.5-6. <https://CRAN.R-project.org/package=vegan>.
- Pahnke, K., & Zahn, R. (2005). Southern Hemisphere water mass conversion linked with North Atlantic climate variability. *Science (New York, N.Y.)*, 307(5716), 1741–1746. <https://doi.org/10.1126/science.1102163>
- R Core Team (2020). R: A language and environment for statistical computing. *R Foundation for Statistical Computing*. <https://www.r-project.org/>
- Rule, S., Brook, B. W., Haberle, S. G., Turney, C. S. M., Kershaw, A. P., & Johnson, C. N. (2012). The aftermath of megafaunal extinction: Ecosystem transformation in Pleistocene Australia. *Science (New York, N.Y.)*, 335(6075), 1483–1486. <https://doi.org/10.1126/science.1214261>
- Russell-Smith, J., Yates, C. P., Whitehead, P. J., Smith, R., Craig, R., Allan, G. E., Thackway, R., Frakes, I., Cridland, S., Meyer, M. C. P., & Gill, A. M. (2007). Bushfires 'down under': Patterns and implications of contemporary Australian landscape burning. *International Journal of Wildland Fire*, 16(4), 361–377. <https://doi.org/10.1071/WF07018>
- Sikes, E. L., & Guilderson, T. P. (2016). Southwest Pacific Ocean surface reservoir ages since the last glaciation: Circulation insights from multiple-core studies. *Paleoceanography*, 31(2), 298–310. <https://doi.org/10.1002/2015PA002855>
- Simoneit, B. R. T. (2002). Biomass burning. A review of organic tracers for smoke from incomplete combustion. *Applied Geochemistry*, 17(3), 129–162. [https://doi.org/10.1016/S0883-2927\(01\)00061-0](https://doi.org/10.1016/S0883-2927(01)00061-0)
- Simoneit, B. R. T., Schauer, J. J., Nolte, C. G., Oros, D. R., Elias, V. O., Fraser, M. P., Rogge, W. F., & Cass, G. R. (1999). Levoglucosan, a tracer for cellulose in biomass burning and atmospheric particles. *Atmospheric Environment*, 33(2), 173–182. [https://doi.org/10.1016/S1352-2310\(98\)00145-9](https://doi.org/10.1016/S1352-2310(98)00145-9)
- Singh, G. (1981). Late Quaternary pollen records and seasonal palaeoclimates of Lake Frome, South Australia. *Hydrobiologia*, 81–82(1), 419–430. <https://doi.org/10.1007/BF00048729>
- Singh, G., & Geissler, E. A. (1985). Lake Cainozoic history of vegetation, fire, lake levels and climate, at Lake George, New South Wales, Australia. *Philosophical Transactions of the Royal Society of London B*, 311, 379–447.
- Singh, G., Kershaw, A. P., & Clark, R. (1981). Quaternary vegetation and fire history in Australia. In A. M. Gill, R. H. Groves & I. R. Noble (Eds), *Fire in the Australian Biota* (pp. 23–54). Australian Academy of Science.
- Sniderman, J. M. K., Hellstrom, J., Woodhead, J. D., Drysdale, R. N., Bajo, P., Archer, M., & Hatcher, L. (2019). Vegetation and climate change in southwestern Australia during the Last Glacial Maximum. *Geophysical Research Letters*, 46(3), 1709–1720. <https://doi.org/10.1029/2018GL080832>
- Spooner, M. I. (2005). *The dynamics of the Leeuwin Current during the middle and late Quaternary* [unpublished PhD thesis]. Australian National University, Canberra.
- Sprigg, R. C. (1947). Submarine canyons of the New Guinea and South Australian coasts. *Transactions of the Royal Society of South Australia*, 71, 296–310.
- Stuut, J-B., Temmesfeld, F., & De Deckker, P. (2014). A 550 kyr record of aeolian activity near North 2014. A 550 ka record of aeolian activity near North West Cape, Australia: Inferences from grain-size distributions and bulk chemistry of SE Indian Ocean deep-sea sediments. *Quaternary Science Reviews*, 83, 83–94. <https://doi.org/10.1016/j.quascirev.2013.11.003>
- Ter Braak, C. J. F., & Juggins, S. (1993). Weighted averaging partial least squares regression (WA-PLS): An improved method for reconstructing environmental variables from species assemblages. *Hydrobiologia*, 269–270(1), 485–502. <https://doi.org/10.1007/BF00028046>
- van de Geer, G., Heusser, L. E., Lynch-Stieglitz, J., & Charles, C. D. (1994). Paleoenvironments of Tasmania inferred from a 5–75 Ka marine pollen record. *Palynology*, 18(1), 33–40. <https://doi.org/10.1080/01916122.1994.9989437>
- van der Kaars, S., & De Deckker, P. (2002). A Late Quaternary pollen record from deep-sea core Fr10/95-GC17 offshore Cape Range Peninsula, northwestern Western Australia. *Review of Palaeobotany*

- and *Palynology*, 120(1–2), 17–39. [https://doi.org/10.1016/S0034-6667\(02\)00075-1](https://doi.org/10.1016/S0034-6667(02)00075-1)
- van der Kaars, S., Miller, G. H., Turney, C. S. M., Cook, E. J., Nürnberg, D., Schönfeld, J., Kershaw, A. P., & Lehman, S. T. (2017). Humans rather than climate the primary cause of Pleistocene megafaunal extinction in Australia. *Nature Communications*, 8, 14142. <https://doi.org/10.1038/ncomms14142>
- von der Borch, C. C. (1968). Southern Australian submarine canyons: Their distribution and ages. *Marine Geology*, 6(4), 267–279. [https://doi.org/10.1016/0025-3227\(68\)90019-4](https://doi.org/10.1016/0025-3227(68)90019-4)

## Supplementary information to accompany the paper entitled:

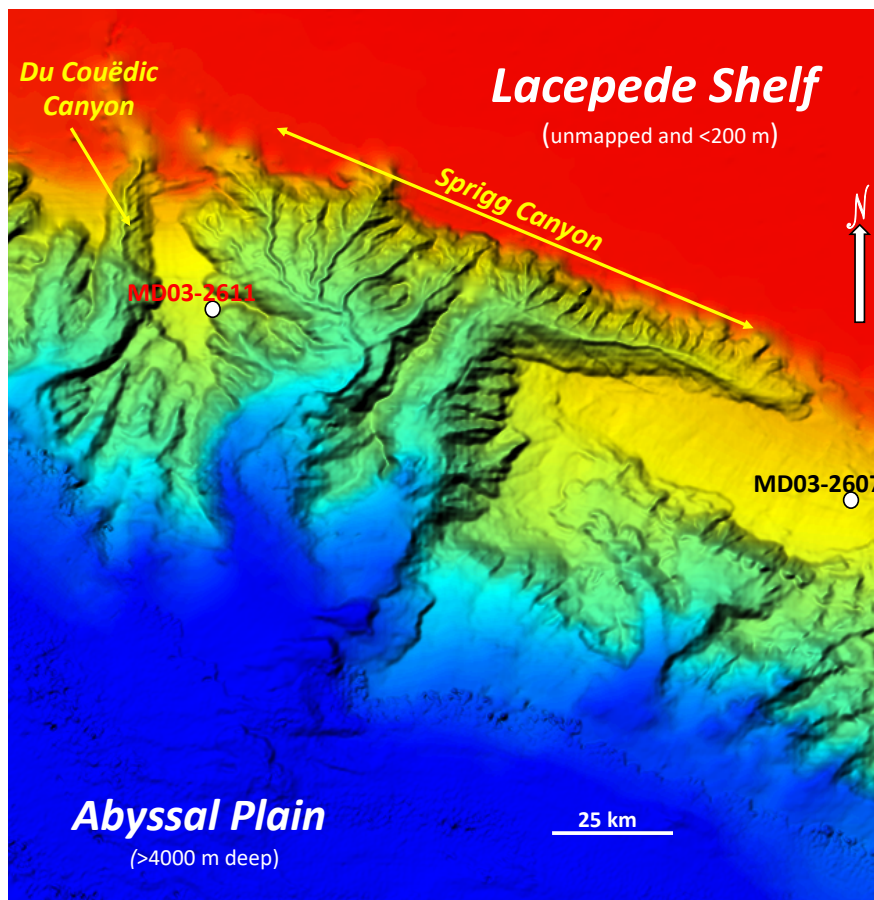
### The pollen record of marine core MD03-2607 offshore Kangaroo Island spanning the last 125 kyears; implications for vegetation changes across the Murray-Darling Basin

Patrick De Deckker<sup>a</sup>, Sander van der Kaars<sup>b,c</sup>, Simon Haberle<sup>d,e</sup>, Quan Hua<sup>f</sup>, Jan-Berend W. Stuut<sup>g</sup>

<sup>a</sup>Research School of Earth Sciences, The Australian National University, Canberra ACT2601; <sup>b</sup>School of Earth, Atmosphere and Environment, Monash University, Clayton VIC 3800; <sup>c</sup>Department of Earth Sciences, Vrije Universiteit Amsterdam, 1081 HV Amsterdam, The Netherlands; <sup>d</sup>School of Culture, History and Language, The Australian National University, Canberra ACT 2601; <sup>e</sup>ARC Centre of Excellence for Australian Biodiversity and Heritage, The Australian National University, Canberra ACT 2601, <sup>f</sup>Australian Nuclear Science and Technology Organisation, Lucas Heights, NSW 2234, Australia; <sup>g</sup>NIOZ - Royal Netherlands Institute for Sea Research, and Utrecht University, 1797 SZ Den Hoorn, Texel, The Netherlands.

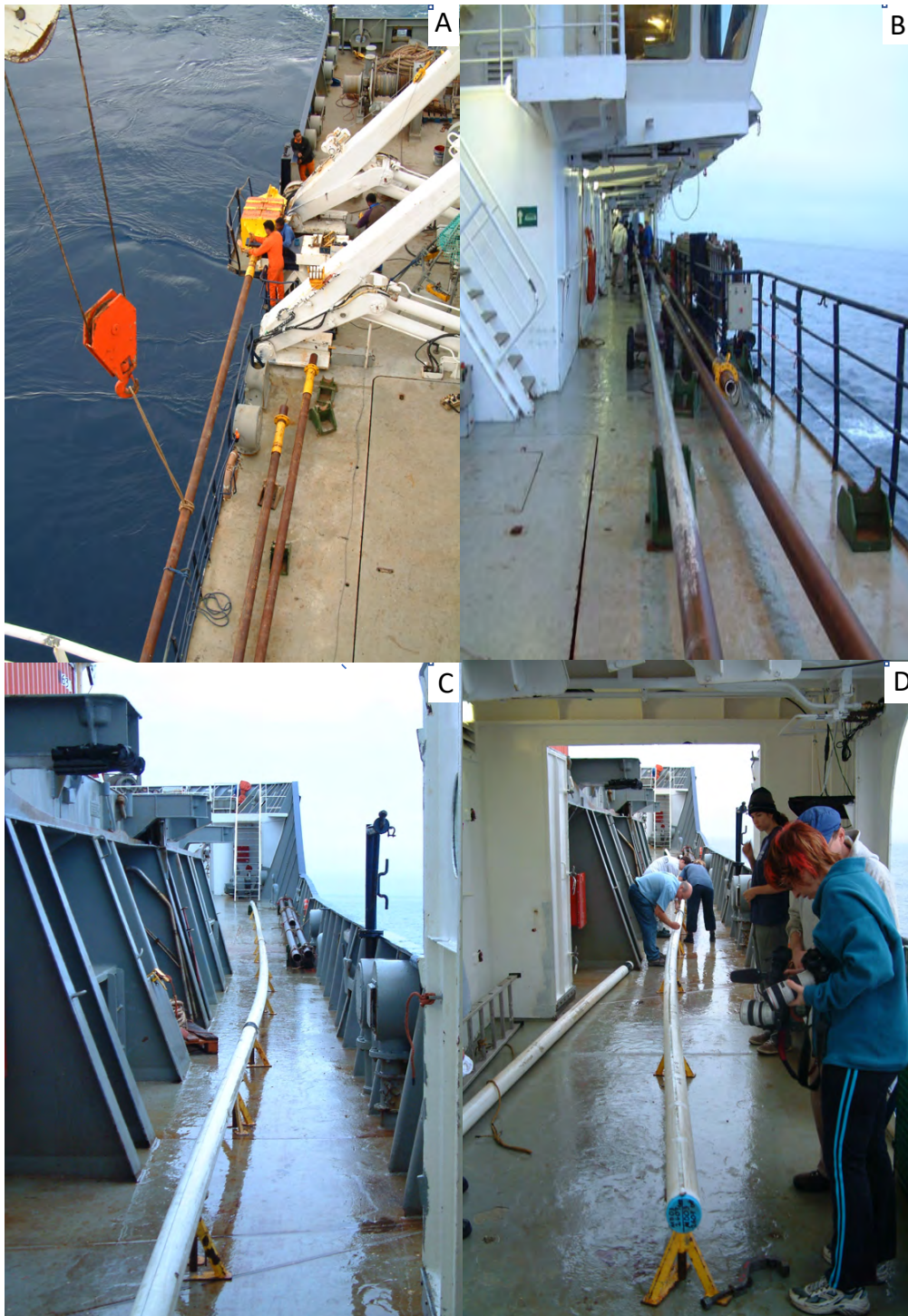
#### 1. Description of core MD03-2607

Calypso core MD03-2607 was taken on February 21, 2003 with the RV *Marion Dufresne* during the AUSCAN campaign (Hill and De Deckker, 2004) on a flat platform east of Sprigg Canyon (Suppl. Fig. 1) southeast of Kangaroo Island. Its location is 36° 57.64' S, 137°E 24.39' and in 865m water depth. The core is 32.95 m long, with the upper 14.7 m (of interest here) consisting of massively bedded fine to very fine (foraminiferal) sands with minor colour variation from darker to paler olive grey. In this upper section of the core occasional zones of irregular or wavy cm-scale darker and lighter layers occur. Below 14.7m the sediments are finer textured.



**Supplementary figure 1.** Tilted 3-D image showing a close up of the Sprigg Canyon and the adjacent du Couëdic Canyon located offshore the Lacepede Shelf (shown in red). The location of the two cores discussed in this paper is shown. Note that empty/hollow meanders are clearly visible in both canyons, suggesting that they are still active today. Image provided by Sharon Glasgow.

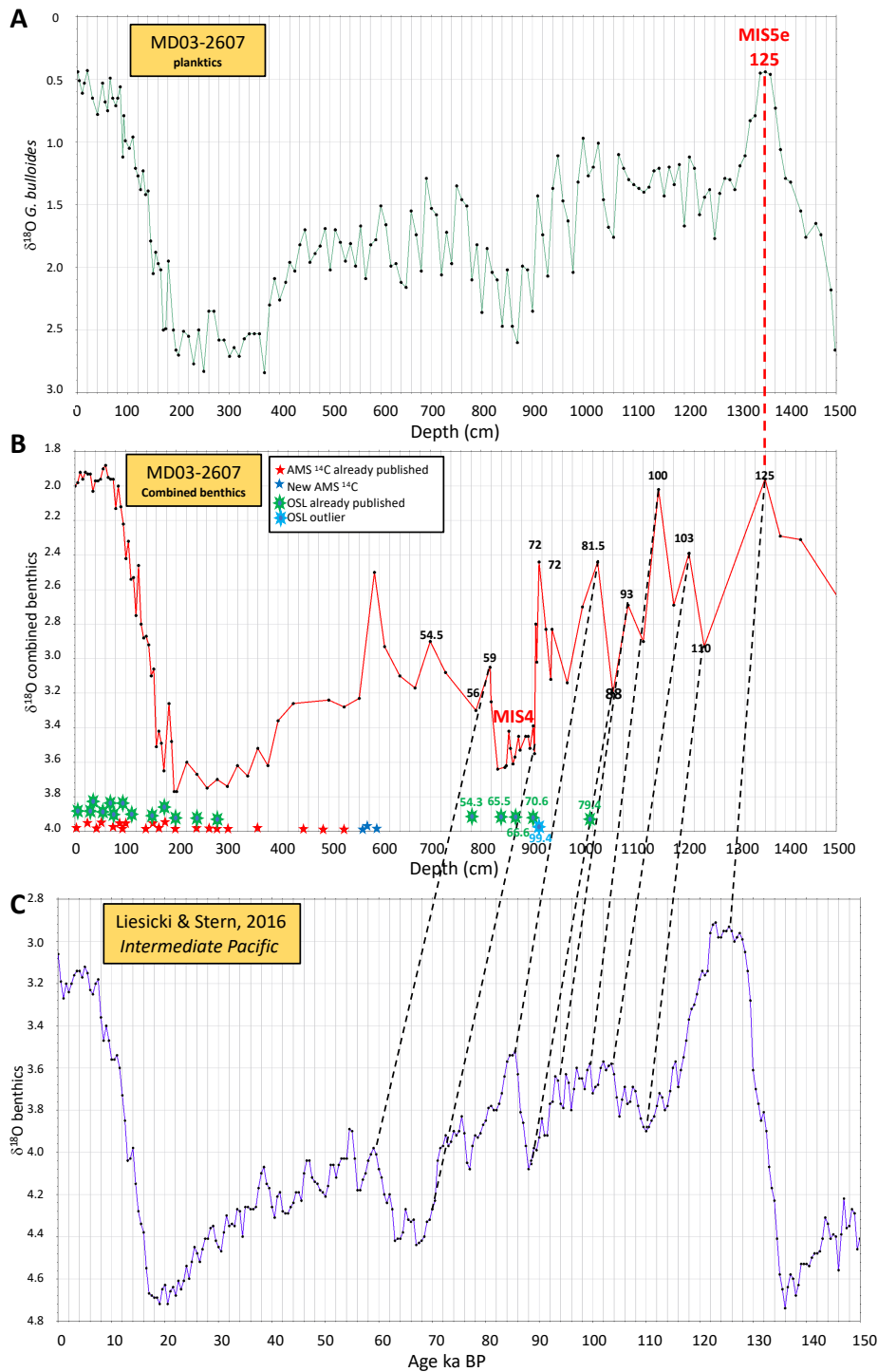
## 2. Photographic record of coring activities on board the *RV Marion Dufresne*



**Supplementary figure 2.** Photographs taken on the *RV Marion Dufresne* showing various activities linked to the retrieval of core MD03-2607. **A:** The 40 m long metal barrel of the Calypso corer is hanging over the side of the ship and is attached to the 800 kg lead weight (painted yellow) before being brought back on the side deck; **B:** The metal barrel inside which core MD03-2607 made of PVC is in the process of being extracted. Note the grey mud on the side of the barrel shows the extent of penetration into the sea floor. Other metal barrels lie on the side deck, ready for the next coring operation; **C:** a large portion of the PVC pipe has already been extracted from the metal barrel and lies on small supports along the front of the ship that is ~120 m long; **D:** people are in the process of labelling the PVC pipe that is to be cut into 1.5 m sections. Eventually each section will be split open lengthwise on board and various measurements will be made soon afterwards, such as sediment logging, colourimetry, magnetic measurements and small samples extraction for microscopic examination. For additional information and photographs, refer to the report made by Hill and De Deckker (2004).

### 3. Core chronology

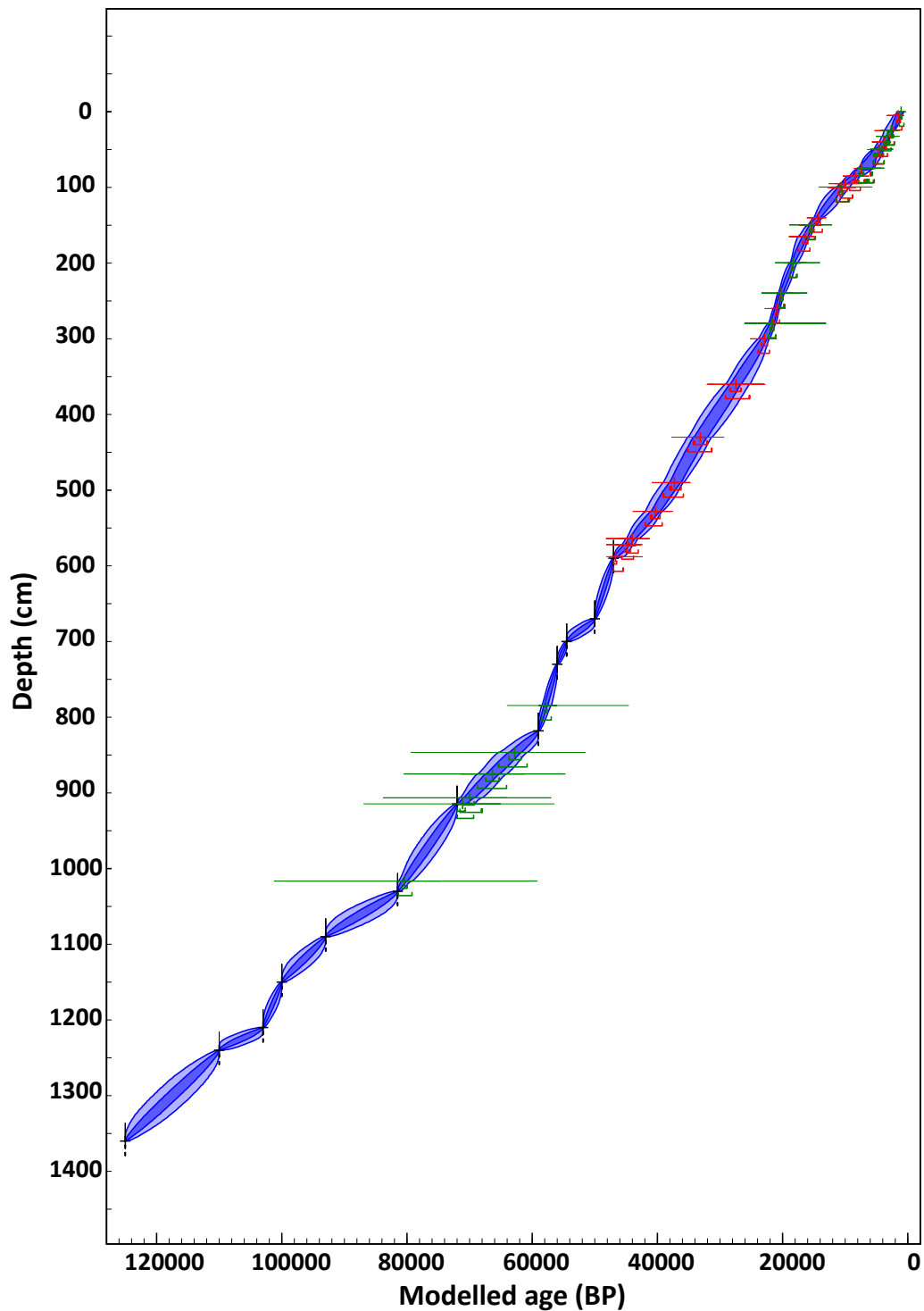
The figures below show the approach taken to obtain a sound chronology for core MD03-2607.



**Supplementary figure 3.** Correlation between various  $\delta^{18}\text{O}$  curves that were used to provide tie points for dating older parts of core MD03-2607. **A:** The  $\delta^{18}\text{O}$  of the planktic foraminifera *G. bulloides* from core MD03-2607 help confirm the culmination of MIS5e at 125 ka; **B:** the  $\delta^{18}\text{O}$  record of a combination of benthic foraminifera obtained from Lopes dos Santos et al. (2013a) and De Deckker et al. (2019). In addition, all the position of all the AMS radiocarbon dates taken from the core are shown as red stars (taken from Lopes dos Santos et al. (2012), with three new ones shown as blue stars. In addition, the position on the core where OSL samples were taken are shown as green stars (taken from Lopes dos Santos et al. (2012) with the ages for the critical samples in the middle portion of the core shown with one outlier shown in pale blue (taken from De Deckker et al., 2019); **C:** the  $\delta^{18}\text{O}$  of benthic foraminifera stack curve (Liesicki and Stern, 2016) for Intermediate Waters for the Pacific Ocean. The dotted lines link respective steps from Liesicki and Stern (2016) that show the tie points and respective ages used to provide ages. All these ages were then used to model the ages for the lower part of the core as shown in Supp. Fig. 4.

#### 4.Age model

The figure below shows the age model calculated for the entirety of the core.

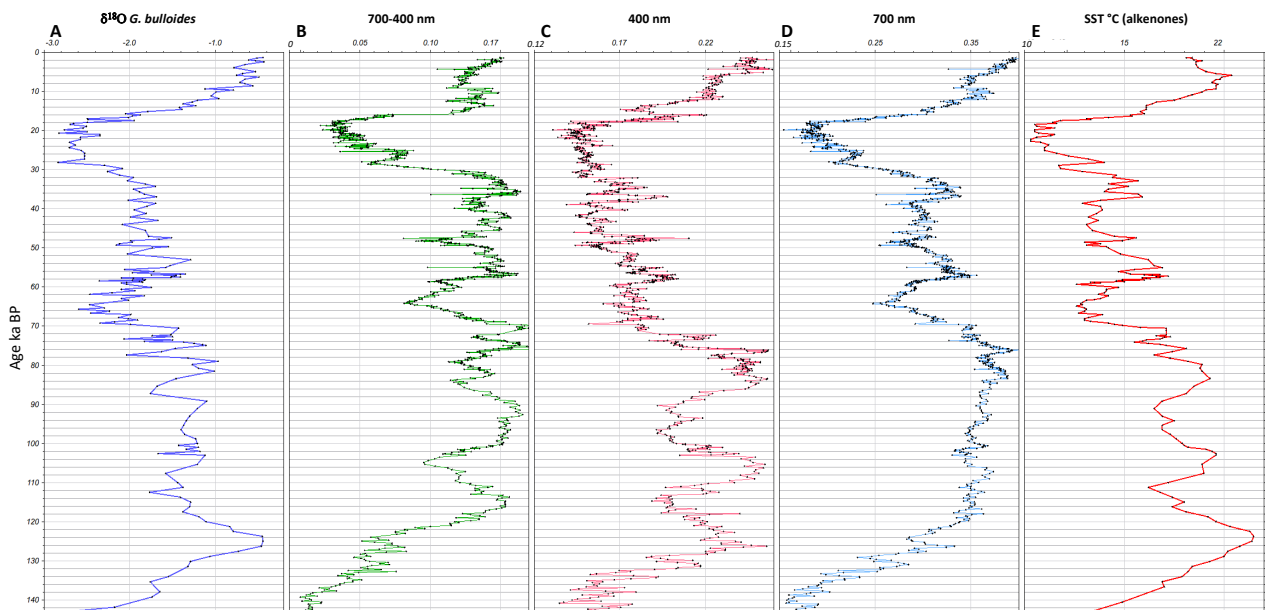


**Supplementary figure 4.** Age-depth model for core MD03-2607 using Bayesian OxCal P sequence (deposition sequence) with variable deposition rate ( $k$ ). A general outlier analysis (prior probability = 0.05). The SHCal20 (Hogg et al., 2020) calibration curve was used for age calibration of the <sup>14</sup>C dates, which were corrected for radiocarbon marine reservoir ages. The OSL and <sup>14</sup>C dates are shown in green and red, respectively. Meanwhile, tie points position linked to the Liesicki and Stern (2016) curve for the Central Water Mass in the western Pacific Ocean shown in Suppl. Fig. 3 appear in black. The list of dates and tie points is provided in Suppl. Table 2.

## 5. Colour reflectance

Colour reflectance of the entire core was obtained following the technique applied by Lourens (2004) to deep-sea cores in the Mediterranean Sea. The measurements, carried out on the ship soon after the opening of the cores, clearly support this observation. A Minolta CM-508 spectrophotometer was used. Measurements were made every cm for the upper 10.5 m of the core and below that this was done at 2 cm intervals.

The profile obtained from the subtraction of the 700 and 400 nm wavelengths in the colour spectrum presented in Suppl. Fig. 5B, in combination with the 400 nm wavelength curve shown in Suppl. Fig. 5C, clearly points out to the similarity of the  $\delta^{18}\text{O}$  of the planktic foraminifer *G. bulloides* presented in Suppl. Fig. 5A - as well the SST reconstructed curve seen in Suppl. Fig. 5E - confirm that the core does not have any hiatus.



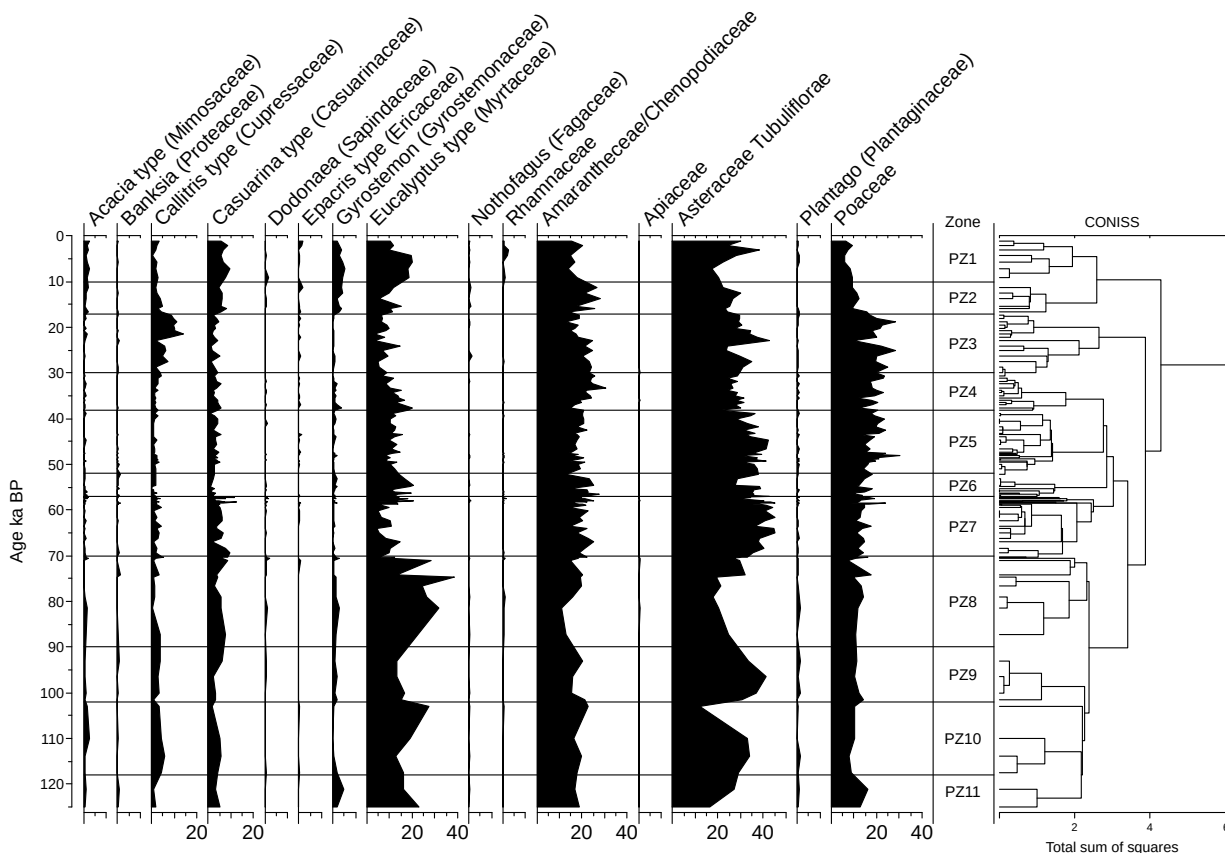
**Supplementary figure 5.** Correlation between various spectral colour reflectance spectra measured on core MD03-2607 soon after opening the core on the ship, against other proxies from the same core such as the  $\delta^{18}\text{O}$  of foraminifera as an indicator of sea level changes, and sea-surface temperature obtained by alkenometry. **A:** The  $\delta^{18}\text{O}$  of the planktic foraminifera *G. bulloides*; **B:** Subtraction of the 700 and 400 nm wavelengths in the colour spectrum measured on the core; **C:** the 400 nm wavelength; **D:** the 700 nm wavelength; **E:** the SST record (Lopes dos Santos et al. (2013b) and De Deckker et al. (2019)). All these curves clearly show that there is no hiatus in the core, nor major turbidite.

## 6. Comparison between the pollen zonation and the marine isotope stages zonation

Suppl. Fig. 6 shows the zonations obtained for the pollen assemblages (PS1 to PZ11) using the arbitrary CONISS routine in TILIA (Grimm, 1987) and the Marine Isotope zonation following the standard nomenclature used by Liesicki and Stern (2016). Note that there is a good overall concordance between the two zonations with the exception of MIS3 that is subdivided into three pollen zones (PZ4 to PZ6). Additionally, the boundaries between MIS3/4 and MIS5d/MIS5e are slightly offset from the pollen zones but the differences are only of the order of 1 millennium or so and may well be caused by the absence of pollen counts for those horizons.



A diagram showing the output of the CONISS routine is provided in Supp. Fig. 7 and this routine places the main division in the diagram between pollen zones 2 and 3. This boundary is calculated on the basis of the greatest dissimilarity between zones using the taxa in this diagram only. The next division is indicated to occur between zones 3 and 4 and the following between zones 7 and 8. These divisions correspond fairly well with the MIS stages placed on the pollen diagram (see Supp. Fig. 6), especially for the latter two divisions (e.g. 3-4 and 7-8).

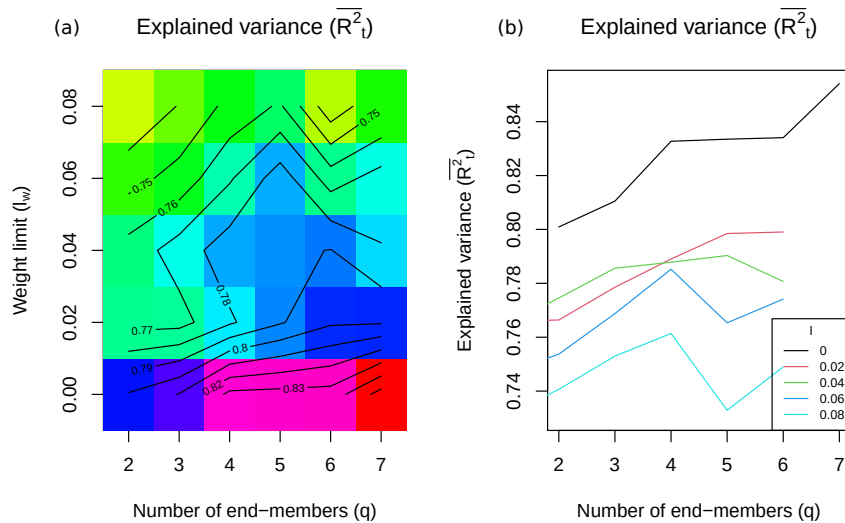


**Supplementary figure 7.** Routine diagram generated by the CONISS program that shows the hierarchy generated for the 120 pollen samples obtained from core 2607.

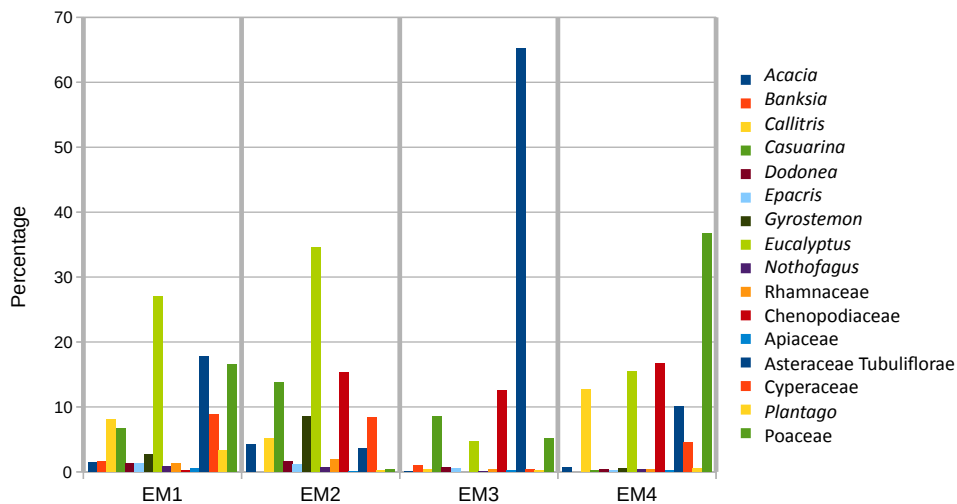
### 7. Clarifying the pollen signal in core 2607 using EMMAgeo

Pollen assemblages obtained from marine cores may have complex signatures because they may have been sourced from different geographic areas as well as from different environments within those areas. In order to attempt to clarify the different source areas, and potentially improve the interpretation of the pollen data from core 2607, the End Member Modelling program using EMMAgeo (Dietze and Dietze, 2019, Dietze et al., 2012) was undertaken in R (R Core Team, 2020). The pollen data were decomposed with the inversion algorithm for 'end-member modelling of compositional data' using EMMAgeo to construct a mixing model that expresses the observations as mixtures of a limited number of end-members. In the modelling stage, the 'mixing problem' is solved in two stages:

(1) The first modelling stage involves the estimation of optimal number ( $q$ ) of end-members and weight loadings ( $l$ ). This estimation is based on output from EMMAgeo that provides the mean/median coefficient of determination ( $r^2$ ) for combinations of  $q$  and  $l$ , and it represents the proportions of the variance explained for each variable (pollen taxon) that can be reproduced by the approximated data (Suppl. Fig. 8).



**Supplementary figure 8.** (a) Mean total  $Rt_2$  (explained variance) of all combinations of weight transformation limits ( $l$ ) and number of end-members ( $q$ ) and (b) of end-members ( $q$ ) at selected weight transformation limits ( $l$ ) from the output of EMMAgeo analysis of 16 selected pollen taxa from core 2607.



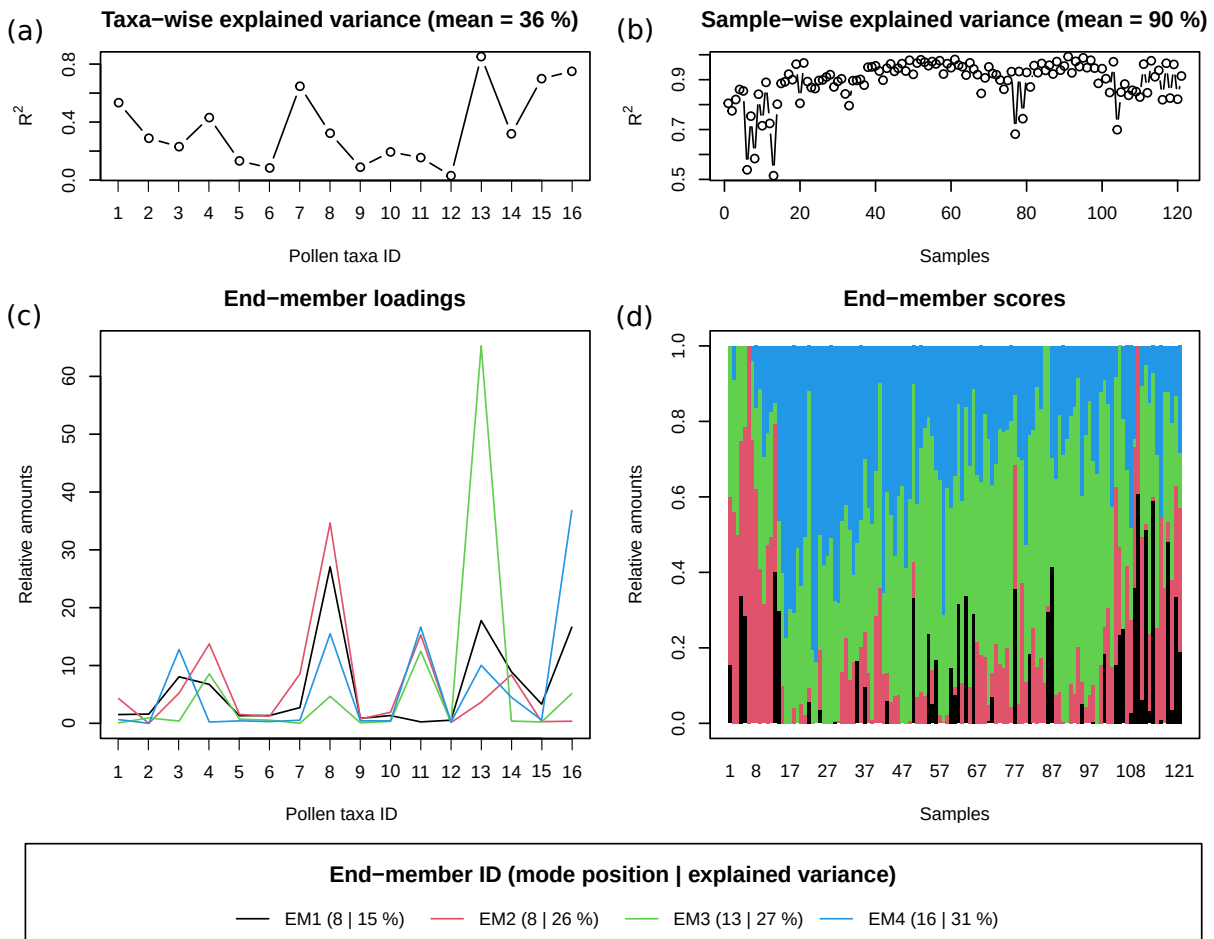
**Supplementary figure 9.** Histograms showing the composition of the 4 end-members resulting from modelling by EMMAgeo of 16 selected pollen taxa from core 2607.

The outcomes show that under different loadings the more robust models are generally achieved when using 4 end-members and that overall a weight loading of 0 produces more robust models;

(2) The second modelling stage involves estimation of the end-member compositions (disentangling and redistribution of pollen percentage data from 16 selected taxa from core 2607 over the 4 end-members) (Suppl. Figs. 9 and 10c), and subsequently, calculation of the proportional contribution of the end members at all core depths (Suppl. Fig. 10d). These end members – extreme, theoretical pollen assemblages - are representative of different types of vegetation and potential source areas.

We also used existing transfer functions from Cook and van der Kaars (2006) to reconstruct annual rainfall, summer rainfall and winter rainfall for each of the vegetation types, identified as EM1 to EM4. These are presented in Supplementary Table 1.

It is noteworthy that vegetation type EM4 (see Supp. Fig. 10) is by far the most arid of the four types. This type is sourced from the Murray sub-basin or, perhaps, it is the vegetation growing on the Lacepede Shelf when exposed during low sea level. We know from observations made at sea when surveying the Lacepede Shelf (P. De Deckker, personal observation during *Southern Surveyor* cruise SS02-06) that a large part of the entire shelf is currently covered with reworked red sand of dunal origin.



**Supplementary figure 10.** Graphical output of the EMMAgeo analysis using 16 selected pollen taxa with number of end-members set at 4 and weight transformation set at 0. (a, b) Measures of model performance (i.e. pollen taxa- and sample-wise  $R^2$ ) (squared Pearson correlation coefficients), (c) end-member loadings of individual pollen taxa and (d) end-member scores. The legend presents the main mode positions (pollen taxon ID) and explained variance of each end-member (%). Pollen taxa IDs are as follows. 1: *Acacia*, 2: *Banksia*, 3: *Callitris*, 4: *Casuarina*, 5: *Dodonaea*, 6: *Epacris*, 7: *Gyrostemon*, 8: *Eucalyptus*, 9: *Nothofagus*, 10: Rhamnaceae, 11: Chenopodiaceae, 12: Apiaceae, 13: Asteraceae Tubuliflorae, 14: Cyperaceae, 15: *Plantago*, 16: Poaceae.

## 8. Comparison with other long pollen records from marine cores offshore Australia

### Core E55-1 offshore Victoria

This core was taken at a water depth of 2,346 m to the west of the Otway Ranges (Fig. 1) and some 37 samples were analysed by Harle (1997) for the period that covered the last glacial/interglacial cycle. Unfortunately, the Holocene sequence was missing in that core due to a mud flow. By linking

the core to an oxygen isotope stratigraphy carried out by Passlow et al. (1997) it was possible to provide a chronology, which then enabled comparison of the pollen record with other sequences in Victoria that relied on poor and/or extrapolated ages. Harle (1997) clarified that the palynoflora for MIS5e represented the wettest phase in contrast to the equivalent of MIS5c on land as previously considered by Kershaw et al. (1991) and Kershaw and Nanson (1993). The work also discussed the mode of transport of the pollen and spores retrieved from core E55-6 and argued that the majority of the pollen was transported by wind, but certain taxa had been transported by water such as fern spores, aquatics and myrtaceous shrubs (that have a limited dispersal range, *sic* Harle, 1997). It was also argued that some rainforest taxa such as *Lagarostrobos* and *Phyllocladus* may have been transported from as far as Tasmania, where they are restricted today, but the predominant wind direction would not favour this. Either these taxa occurred in western Victoria or were transported by an oceanic current such as the Flinders Current that travels northward along the western coast of Tasmania (Richardson et al., 2019). Major findings of relevance to the study of core 2697 are: (1) *Callitris* is restricted to MIS 2 and 5d and this parallels our findings on core 2607; (2) *Eucalyptus* counts are highest during the entire MIS 5 (and in particular MIS 5c) and this coincided also with high charcoal counts. In contrast, charcoal counts were also low during MIS 2 as seen in our work in core 2607; and (3) Asteraceae (spiny and spineless) counts fluctuated in discordance with Poaceae pollen, but the trend is opposite to that found in core 2607. During MIS 2, when *Callitris* representation is high (only one sample), *Eucalyptus* is low.

#### **Core SO36-7SL offshore western Tasmania**

This core was taken at a water depth of 1,085 m (Fig. 1) and extends as far back as 75 ka BP. A total of 44 samples were analysed and are compared against a  $\delta^{18}\text{O}$  curve obtained from benthic foraminifera compared against the astronomically tuned time scale established at that time by Martinson et al. (1987). In contrast with the findings from core 2607 and E55-6, rainforest taxa are recognised in all samples, but percentages decreased for MIS stages before the Holocene. The surprise was to find the highest counts of *Lagarostrobos* (commonly known as Huon Pine) during MIS 2. This may have been due to lateral transport conditions at sea since the algae *Botryococcus* and *Pediastrum* were recorded in all samples and these would indicate fluvial transport from inland. *Lagarostrobos* pollen may have been transported to the core site with the Flinders Current since it is most common in SW Tasmania (refer to details discussed for core E55-6, above).

During the warm phases (MIS 5a, 3 and 1) *Eucalyptus* numbers were notably high whereas they were lower during the cold phases (MIS 2 and 4) and it is during those times that grasses numbers peaked. We assume that the alpine/subalpine flora, consisting of herbs and woodland/shrub, would have expanded during the glacial phases. No charcoal counts were reported in the pollen diagram.

The success story of this core is that it permitted a good correlation with pollen records (published at that time) from inland sequences, many of which had gaps for the period spanning 75 ka; this was the same 'achievement' for core E55-6.

#### **Core Fr1/94-GC3**

This core was taken on the East Tasman Plateau at a water depth of 2,667 m. With a length of only 4.71m, it is very short for a marine core but the sediment sequence is very condensed, spanning the last 460 ka BP. Only 29 samples cover the last glacial/interglacial cycle, but the advantage of this core record is that it has been possible to compare the last cycle with the 3 previous ones. The core location, on the East Tasman Plateau, is separated from the Tasmanian mainland by a deep trough (see Fig. 1 in De Deckker et al, 2019a) and, consequently, in contrast with the other cores mentioned above, there was no fluvial transport that would have brought pollen to the core site.

The chronology of this core is based on a planktic and benthic  $\delta^{18}\text{O}$  stratigraphy, so ages are well defined. A variety of proxies was studied from the core, enabling comparison of the pollen record with SST using 3 different techniques (see De Deckker et al., 2019b), as well as estimated seasonal patterns of rainfall and temperature on land.

The salient features interpreted from the pollen record covering the last glacial/interglacial cycle are: (1) alpine taxa are better represented during MIS stages 2 and 4, and late in MIS 3; (2) rainforest taxa were best represented during MIS 5, and to a lesser extent during MIS 3; (3) overall *Eucalyptus* numbers were consistently low during MIS 2, 4 and 6; (4) *Callitris* pollen is absent in that core, implying wetter conditions than on the Australian mainland; and (5) estimates of rainfall on land (obtained from the pollen record) show drying through the record through time and land temperatures reconstructed from the pollen record indicate a temperature rise during MIS 2 which is opposite to the reconstructed sea-surface temperatures. This latter feature is rather puzzling and will need to be revisited, especially since too few samples were used for those reconstructions. Comparing the records from Fr1/94-GC3 and core SO36-7SL, we see almost no alpine taxa in the former during MIS4 while alpine taxa increase in the latter during the same time period. However, there were too few samples to come to a definite answer. In summary, the alpine shrubland and grasses expanded during MIS 2 and 4 (as well as 6 in core GC3).

#### **Core Fr10/95-GC17 offshore NW Western Australia**

This core is located on the Exmouth Plateau offshore North West Cape at a water depth of 1093 m. It is located in the subtropics and the salient feature is that, during monsoonal activity, vast amounts of fluvial clays were transported to the ocean. This is reflected in the Holocene sediments by the colour of the upper 88 cm of the sediment which is yellowish brown (10 YR 4/3 on the Munsell Soil Chart). In the lower part of the core, the sediment is coloured olive-grey [7.5Y 5/2]. Obviously, pollen can be transported at sea during the floods, but an aeolian component also must have also prevailed, especially when monsoonal rains would have been absent as shown by the occurrence of airborne clays in the core (Gingele et al., 2001). van der Kaars and De Deckker (2002) and van der Kaars et al. (2006) examined the pollen record of this core spanning a record of 100 ka, with an unfortunate gap recorded from 60 to 46 ka BP. Interpretation of this pollen record varies considerably from the other core sites discussed above due to the different vegetation types in northwestern Western Australia. De Deckker et al. (2014) re-examined the pollen record for the period spanning the last 34 ka, in conjunction with several other proxies, such as SST reconstruction, monsoonal activity, changes in oceanic productivity and stratification and airborne clays deposited at sea. In that same paper, temperature and rainfall on land were reconstructed from the pollen data based on the work of van der Kaars et al. (2006) and compared with conditions at sea. Importantly, the presence of spores in all the samples in the core inform on the behaviour of the Leeuwin Current (that parallels the coast), bringing pteridophyte spores from as far as Indonesia and/or New Guinea during the second half of the Holocene. Based on the work of van der Kaars and De Deckker (2002), salient vegetational features are that *Callitris* is highest during the LGM (as observed in core 2607 in this present study), with fewer numbers during the middle of the Holocene, part of MIS 3 and commonly occurring during the 95 to 65 ka period. Since the LGM, *Eucalyptus* increased progressively but was never as high as lower down in the core (viz. part of MIS 3 and during the 100 to 65 ka period). Once again, there is good correspondence between the *Eucalyptus* and charcoal (as we note in core 2607).

Noticeable also are the fluctuating levels of Poaceae and Asteraceae/Tubiflorae: high (~30%) Poaceae and low (~20%) Asteraceae/Tubiflorae that coincide with predominantly summer rainfall that resulted from monsoonal activity after 13 ka BP. This is in contrast with the LGM and before (De Deckker et al., 2014) when conditions were very different. Alternating levels between those taxa during the second half of the Holocene are likely the result of alternating and

contrasting conditions set by ENSO that was in full force during the last 6,000 years (see Perner et al. (2018) for more information). Lastly, the appearance in the record of mangrove pollen (Rhizophoraceae and *Avicennia*) during the Holocene likely represents stabilization of the coastline, and declines after 6 ka BP as already found by Grindrod et al (1999) for other coastal sites in northern Australia.

### ***Core ODP 820A offshore Queensland adjacent to the Great Barrier Reef***

This core was obtained from ODP site 820A at a water depth of 278 m and is adjacent to the humid tropics of northern Australia. It is situated seaward of the Great Barrier Reef on the continental slope, about 40 km from the modern-day coast and about 100 km from Lynch's Crater, a site with an extensive and very detailed pollen record (Kershaw, 1981, 1986; Kershaw et al., 1991, 2007). The palynofloral record of this core is very different from the others mentioned here as it relates to tropical forests dominated by gymnosperm and angiosperm rainforests. Despite that, and the fact that the  $\delta^{18}\text{O}$  record of foraminifera for this core is problematic (further discussed below) several distinct trends are noticeable. During the LGM, when sea level had dropped between 124 and 128 m at 20.05 ka BP (Yokoyama et al., 2018), sandy layers are clearly visible in the core (~7.25 m with 60% sand wt%). These resulted from the shallowness of the core site and the same occurs again at ~33 m core depth (Peerdeman and Davies, 1993). These levels correspond to MIS 2 and 6, respectively. In addition, Peerdeman et al. (1993) also mentioned two hiatuses in the upper part of the core (at 8.02 to 12.1 m and 35.55 to 35.8 m) which they argue indicate the absence of MIS 4 and 7. However, further examination of the  $\delta^{18}\text{O}$  curve displayed in figure 2 in Moss and Kershaw (2000) shows the typical MIS4 shift (OIS4 *sic* in Moss and Kershaw (2000) and it is surprising to see high rainforest gymnosperm counts coinciding with this episode. This further confirms that during MIS4 northern Australia was considerably wetter than was previously estimated, as argued in De Deckker et al. (2020), and also refer to the estimated evapotranspiration potential in central Australia argued by Miller et al. (2016) for this period (discussed in De Deckker et al., 2020).

At first glance, it appears that the percentage of rainforest gymnosperm taxa were much higher during MIS3 compared to MIS1, and during the LGM sclerophyll herbs made up over 65% of the total palynoflora. As might be expected, glacial conditions affected the vegetation inland. The sandy layer at ~33 m that is representative of MIS 6 had fewer sclerophyll herbs. It could be that reworked sands affected the palynoflora taphonomy resulting from a low sea level stand. Similarly, the peak of *Eucalyptus* preceding the low sea level in Moss and Kershaw (2007; zone 3 in fig. 2) coincides with the highest peak of charcoal recorded in the core. The previous high peak occurs exactly during MIS6 in the sandy layers. Following both charcoal peaks, the mangrove pollen increased rapidly, coinciding each time with a period of marine transgression (refer to discussions in Moss and Kershaw (2013)). Also, aquatic pollen abounds at all levels in the core, not surprising since the core site is so close to the Queensland coast, and an aspect that must be taken into account concerning the origin of the palynoflora. It is possible that the palynoflora recorded at site 820A may have come from the north by ocean currents rather than having been blown offshore from the adjacent Atherton Tablelands where rainforest does grow today, although in reduced areas due to European land clearance (Moss et al., 2017).

The revised chronology of the upper 22 m of the ODP820 record is based on 14 AMS  $^{14}\text{C}$  dates on pollen concentrates down to 16 m bsf, and closely aligns the palynomorph events recognised in the core with those identified in terrestrial records in the region (Kershaw et al., 2007). The revised chronology makes it clearer that MIS3 was generally wetter than previously thought and MIS 2 was dry and was followed by climatic amelioration during the Holocene. We note that, at the end of MIS4 as shown in Moss et al. (2013, figs. 3, 4), high percentages of rainforest taxa are present, further confirming that MIS4 was wet in northeastern Australia. Nevertheless, caution is required as humans were likely around and may have affected vegetation through burning.

**Supplementary Table 1.** Reconstruction of estimated rainfall for the four vegetation type end-members. ANRF = annual rainfall, SUMRF = summer rainfall and WINRF = winter rainfall. See text for further details.

	ANRF	SUMRF	WINRF
<b>EM1</b>	732	100	298
<b>EM2</b>	652	69	263
<b>EM3</b>	725	109	255
<b>EM4</b>	394	78	109

**Supplementary Table 2.** List of all the ages used to construct the age model for core MD03-2607

	Type of dating	Depth (cm)	pMC		$\delta^{13}\text{C}$ (‰ PDB)		$^{14}\text{C}$ Age (kBP)		R ( $^{14}\text{C}$ kyr)	R-corrected $^{14}\text{C}$ Age (kBP)		Calendar Age (ka) *		Comments
			mean	1 $\sigma$	mean	1 $\sigma$	mean	1 $\sigma$		mean	1 $\sigma$	mean	error	
1	OSL	0										1.070	0.160	
2	$^{14}\text{C}$	5	73.1	1.73	-0.5	0.2	2.600	0.190	0.440	2.160	0.190	1.560	0.670	
3	OSL	24.5										2.380	0.410	
4	$^{14}\text{C}$	25	61.38	1.37	0.0	0.2	4.010	0.180	0.440	3.570	0.180	2.780	0.820	
5	OSL	32.5										3.110	0.670	
6	$^{14}\text{C}$	40	61.12	1.42	0.2	0.2	4.045	0.185	0.440	3.605	0.185	3.860	0.670	
7	OSL	49.5										3.940	0.610	
8	$^{14}\text{C}$	50	53.19	1.2	-0.5	0.2	5.155	0.180	0.440	4.715	0.180	4.720	1.070	
9	OSL	63.5										24.060	2.160	discarded due to turbidity current issue
10	OSL	74.5										5.370	0.610	
11	$^{14}\text{C}$	75	41.48	1.01	-0.1	0.2	7.155	0.195	0.440	6.715	0.195	7.130	1.400	
12	$^{14}\text{C}$	85	39.23	0.96	-0.3	0.2	7.600	0.195	0.440	7.160	0.195	8.410	0.980	
13	$^{14}\text{C}$	95	30.13	0.83	-0.3	0.2	9.720	0.220	0.440	9.280	0.220	9.980	0.960	
14	OSL	99.5										9.980	1.610	
15	$^{14}\text{C}$	100	28.41	0.76	-0.4	0.2	10.190	0.215	0.440	9.750	0.215	10.690	0.960	
16	$^{14}\text{C}$	140	20.71	0.53	-1.1	0.2	12.730	0.205	0.600	12.130	0.205	14.330	0.700	
17	OSL	149.5										15.520	1.300	
18	$^{14}\text{C}$	150	18.53	0.51	-0.7	0.2	13.620	0.220	0.600	13.020	0.220	15.420	0.540	
19	$^{14}\text{C}$	165	15.54	0.45	-0.7	0.2	15.040	0.235	0.600	14.440	0.235	16.500	0.940	
20	OSL	174.5										12.750	1.890	discarded due to turbidity current issue
21	$^{14}\text{C}$	175	12.47	0.38	0.0	0.2	16.810	0.240						discarded
22	$^{14}\text{C}$	175	10.44	0.3	0.0	0.2	18.240	0.230						discarded
23	OSL	199.5										17.600	1.360	
24	$^{14}\text{C}$	200	14.07	0.4	0.3	0.2	15.840	0.225	0.600	15.240	0.225	18.350	0.520	
25	OSL	239.5										19.720	1.390	
26	$^{14}\text{C}$	240	11.43	0.34	0.4	0.2	17.510	0.240	0.600	16.910	0.240	20.230	0.500	
27	$^{14}\text{C}$	260	10.74	0.33	-0.4	0.2	18.010	0.245	0.600	17.410	0.245	20.970	0.480	
28	OSL	279.5										19.580	2.480	
29	$^{14}\text{C}$	280	9.95	0.32	0.0	0.2	18.630	0.260	0.600	18.030	0.260	21.730	0.580	
30	$^{14}\text{C}$	300	9.34	0.25	0.4	0.2	19.130	0.215	0.600	18.530	0.215	22.970	0.930	
31	$^{14}\text{C}$	360	7.02	0.33	0.2	0.2	21.420	0.380	0.700	20.720	0.380	27.360	1.910	
32	$^{14}\text{C}$	430	2.17	0.14	0.0	0.2	30.850	0.500	0.700	30.150	0.500	33.180	2.020	
33	$^{14}\text{C}$	490	?	?	?	?	32.600	0.250	0.700	31.900	0.250	37.340	1.740	
34	$^{14}\text{C}$	528	?	?	?	?	35.215	0.275	0.700	34.515	0.275	40.440	1.430	
35	$^{14}\text{C}$	564	0.53	0.04	0.0		42.140	0.630	0.700	41.440	0.630	44.010	0.980	
36	$^{14}\text{C}$	572	0.53	0.04	0.2	0.2	42.090	0.620	0.700	41.390	0.620	44.760	0.940	
37	$^{14}\text{C}$	588	0.53	0.04	0.1	0.1	42.030	0.620	0.700	41.330	0.620	46.530	0.940	
38	$\delta^{18}\text{O}$ tie point	590										47.000		
39	$\delta^{18}\text{O}$ tie point	670										50.000		
40	$\delta^{18}\text{O}$ tie point	700										54.500		
41	$\delta^{18}\text{O}$ tie point	730										56.000		
42	OSL	782-787										54.300	3.700	
43	$\delta^{18}\text{O}$ tie point	818										59.000		
44	OSL	844-849										65.400	5.300	
45	OSL	872-878										67.600	4.900	
46	OSL	904-909										70.400	5.100	
47	OSL	912-917										71.700	5.800	
48	$\delta^{18}\text{O}$ tie point	914.5										72.000		
49	OSL	1014-1019										80.200	8.000	
50	$\delta^{18}\text{O}$ tie point	1030										81.500		
51	$\delta^{18}\text{O}$ tie point	1090										93.000		
52	$\delta^{18}\text{O}$ tie point	1150										100.000		
53	$\delta^{18}\text{O}$ tie point	1210										103.000		
54	$\delta^{18}\text{O}$ tie point	1240										110.000		
55	$\delta^{18}\text{O}$ tie point	1360										125.000		

Note: \* - cal. ages for  $^{14}\text{C}$  samples are shown as modelled mean ages  $\pm 2\sigma$  uncertainties

## References

- Cook, E.J., van der Kaars, S. (2006). Development and testing of transfer functions for generating quantitative climatic estimates from Australian pollen data. *Journal of Quaternary Science*, 21, 723-733. doi.org/10.1002/jqs.1076
- De Deckker, P., Arnold, L.J., van der Kaars, S., Bayon, G., Stuut, J-B.W., Perner, K., Lopes dos Santos, R., Uemura, R., Demuro, M. (2019). Marine Isotope Stage 4 in Australasia: a full glacial culminating 65,000 years ago – global

- connections and implications for human dispersal. *Quaternary Science Reviews*, 204, 187-207. doi.org/10.1016/j.quascirev.2018.11.017.
- De Deckker, P., Barrows, T.T., Rogers, J. (2014). Land–sea correlations in the Australian region: post-glacial onset of the monsoon in northwestern Western Australia. *Quaternary Science Reviews*, 105, 181-194. doi.org/10.1016/j.quascirev.2014.09.030.
- De Deckker, P., Barrows, T.T., Stuut, J.-N., van der Kaars, S., Ayress, M.A., Rogers, J., Chaproniere, G. (2019b). Land-sea correlations in the Australian region: 460k years of changes recorded in a deep-sea core offshore Tasmania. Part 2: the marine compared with the terrestrial record. *Australian Journal of Earth Sciences*, 66, 17-35. doi.org/10.1080/08120099.2018.1495101.
- De Deckker, P., Moros, M., Perner, K., Blanz, T., Wacker, L., Schneider, R., Barrows, T.T., O’loingsigh, T. Jansen, E. (2020). Climatic evolution in the Australian region over the last 94 ka - spanning human occupancy -, and unveiling the Last Glacial Maximum. *Quaternary Science Reviews* 106593. doi.org/10.1016/j.quascirev.2020.106593
- De Deckker, P., van der Kaars, S., Macphail, M., Hope, G. (2019a). Land-sea correlations in the Australian region: 460k years of changes recorded in a deep-sea core offshore Tasmania. Part 1: the pollen record. *Australian Journal of Earth Sciences*, 66, 1-15. doi.org/10.1080/08120099.2018.1495100.
- Dietze, E., Dietze, M. (2019). Grain-size distribution unmixing using the R package EMMAge. *E&G Quaternary Science Journal*, 68, 29–46. doi.org/10.5194/egqsj-68-29-2019.
- Dietze, M., Dietze, E. (2016). EMMAgeo: End-Member Modelling of Grain-Size Data, available at: <https://cran.r-project.org/web/packages/EMMAgeo/>
- Gingele, F.X., De Deckker, P., Hillenbrand, C.-D. (2001). Late Quaternary fluctuations of the Leeuwin Current and palaeoclimates on the adjacent land masses e clay mineral evidence. *Australian Journal of Earth Science*, 48, 867-874. doi.org/10.1046/j.1440-0952.2001.00905.x
- Grimm, E.C. (1987). CONISS: A fortran 77 program for stratigraphically constrained cluster analysis by the method of incremental sum of squares. *Computer Geoscience*, 13, 13-35. doi.org/10.1016/0098-3004(87)90022-7.
- Harle, K.J. (1997). Late Quaternary vegetation and climate change in southeastern Australia: Palynological evidence from marine core E55-6. *Palaeogeography, Palaeoclimatology, Palaeoecology*, 131, 465–483. doi.org/10.1016/S0031-0182(97)00016-3.
- Hill, P., De Deckker, P. (2004). AUSCAN Seafloor Mapping and Geological Sampling Survey on the Australian Southern Margin by RV *Marion Dufresne* in 2003. *Geoscience Australia Record*, 2004/04, 136pp.
- Hogg, A.G., and 14 other authors. (2020). SHCal20 Southern Hemisphere calibration, 0– 55,000 years cal BP. Radiocarbon doi:10.1017/RDC.2020.59.
- Kershaw, A.P. (1981). Climatic change and Aboriginal burning in north-east Australia during the last two glacial/interglacial cycles. *Nature*, 322, 47-49.
- Kershaw, A.P. (1986). Pleistocene vegetation of the humid tropics of northeastern Queensland, Australia. *Palaeogeography Palaeoclimatology Palaeoecology*, 109, 399-412. doi.org/10.1016/0031-0182(94)90188-0.
- Kershaw, A.P., Baird, J.G., D’Costa, D.M., Edney, P.A., Peterson, J.A., Strickland, K.M. (1991). A comparison of long Quaternary records from the Atherton and Western Plains volcanic sequences. *Geological Society of Australia, Special Publication*, 18, 288-301.
- Kershaw, A.P., Bretherton, S.C., van der Kaars, S. (2007). A complete pollen record of the last 230 ka from Lynch’s Crater, north-east Australia. *Palaeogeography, Palaeoclimatology, Palaeoecology* 251, 23-45. doi.org/10.1016/j.palaeo.2007.02.015.
- Kershaw, A.P., McKenzie, G.M., Porch, N., Roberts, R.G., Brown, J., Heijnis, H., Orr, M.L., Jacobsen, G., Newall, P.R. (2007). A high-resolution record of vegetation and climate through the last glacial cycles from Caledonia Fen, southeastern highlands of Australia. *Journal of Quaternary Science*, 22, 481-500. doi.org/10.1002/jqs.1127.
- Kershaw, A.P., Nanson, G.C. (1993). The last full glacial cycle in the Australian region. *Global and Planetary Change*, 7, 1-9. doi.org/10.1016/0921-8181(93)90036-N
- Lisiecki, L.E., Stern, J.V. (2016). Regional and global benthic  $\delta^{18}\text{O}$  stacks for the last glacial cycle. *Paleoceanography*, 31, 1368-1394. <https://doi.org/10.1002/2016PA003002>.
- Lopes dos Santos, R.A., Wilkins, D., De Deckker, P., Schouten, S. (2012). Late Quaternary productivity changes from offshore Southeastern Australia: a biomarker approach. *Palaeogeography, Palaeoclimatology, Palaeoecology*, 363-364, 48-56. doi.org/10.1016/j.palaeo.2012.08.013.
- Lopes dos Santos, R., De Deckker, P., Hopmans, E.C., Magee, J.W., Mets, A., Sinninghe, J.S., Schouten, S. (2013a). Abrupt vegetation change after the Late Quaternary megafaunal extinction in southeastern Australia. *Nature Geoscience*, doi.org/10.1038/NGEO1856.
- Lopes dos Santos, R., Spooner, M. I., Barrows, T.T., De Deckker, P., Sinninghe, J.S., Schouten, S. (2013b). Comparison of organic ( $\text{U}^{K}_{37}$ ,  $\text{TEX}^{\text{H}}_{86}$ , LDI) and faunal proxies (foraminiferal assemblages) for reconstruction of late Quaternary sea surface temperature variability from offshore southeastern Australia. *Paleoceanography*, 28, 1–11, doi:10.1002/palo.20035.

- Martinson, D.G., Pisias, N.G., Hays J.D., Imbrie, J., Moore, T.C., Shackleton, N.J. (1987). Age dating and the orbital theory of the ice ages: development of a high-resolution 0-300,000-year chronostratigraphy. *Quaternary Research*, 27, 1-29. [doi.org/10.1016/0033-5894\(87\)90046-9](https://doi.org/10.1016/0033-5894(87)90046-9).
- Miller, G.H., Fogel, M.L., Magee, J.W., Gagan, M.K. (2016). Disentangling the impacts of climate and human colonization on the flora and fauna of the Australian arid zone over the past 100 ka using stable isotopes in avian eggshell. *Quaternary Science Reviews*, 151, 27-57. [doi.org/10.1016/j.quascirev.2016.08.009](https://doi.org/10.1016/j.quascirev.2016.08.009).
- Moss, P.T., Dunbar, G.B., Thomas, Z., Turney, C., Kershaw, A.P. (2013). A 60000-year record of environmental change for the Wet Tropics of north-eastern Australia based on the ODP 820 marine core. *Journal of Quaternary Science* 32, 704-716. [doi.org/10.1002/jqs.2977](https://doi.org/10.1002/jqs.2977).
- Moss, P.T., Kershaw, A.P. (2000). The last glacial cycle from the humid tropics of northeastern Australia: comparison of a terrestrial and a marine record. *Palaeogeography Palaeoclimatology Palaeoecology*, 155, 155–176.
- Moss, P.T., Kershaw, A.P. (2007). A late Quaternary marine palynological record (Oxygen isotope stages 1-7) for the Humid Tropics of northeastern Australia based on ODP Site 820). *Palaeogeography, Palaeoclimatology, Palaeoecology*, 251, 4-22. [doi.org/10.1016/S0031-0182\(99\)00099-1](https://doi.org/10.1016/S0031-0182(99)00099-1).
- Peerdeman, F.M., Davies, P.J. (1993). Sedimentological response of an outer-shelf, upper-slope sequence to rapid changes in Pleistocene eustatic sea level: Hole 820a, northeastern Australian margin. *Proceedings of the Ocean Drilling Program, Scientific Results*, 133, 303-313. [doi.org/10.2973/odp.proc.sr.133.236.1993](https://doi.org/10.2973/odp.proc.sr.133.236.1993).
- Peerdeman, F.M., Davies, P.J., Chivas, A.R. The stable oxygen isotope signal in shallow-water, upper-slope sediments off the Great Barrier Reef (Hole 820A). *Proceedings of the Ocean Drilling Program, Scientific Results*, 133, 163-172. [doi.org/10.2973/odp.proc.sr.133.288.1993](https://doi.org/10.2973/odp.proc.sr.133.288.1993).
- Perner, K., Moros, M., De Deckker, P., Blanz, T., Wacker, L., Telford, R., Siegel, H., Schneider, R., Jansen, E. (2018). Heat export from the tropics drives mid to late Holocene palaeoceanographic changes offshore southern Australia. *Quaternary Science Reviews* 180, 96-110. [doi.org/10.1016/j.quascirev.2017.11.033](https://doi.org/10.1016/j.quascirev.2017.11.033).
- R Core Team (2020). R: A language and environment for statistical computing. R Foundation for Statistical Computing, Vienna, Austria. URL <https://www.R-project.org/>
- Richardson, L.E., Middleton, J.F., Kyser, T.K., James, N.P., Opdyke, B.N. (2019). Shallow water masses and their connectivity along the southern Australian continental margin. *Deep-Sea Research Part I*, [doi.org/10.1016/j.dsr.2019.103083](https://doi.org/10.1016/j.dsr.2019.103083).
- van der Kaars, S., De Deckker, P. (2002). A Late Quaternary pollen record from deep-sea core Fr10/95-GC17 offshore Cape Range Peninsula, northwestern Western Australia. *Reviews in Palaeobotany and Palynology*, 120, 17-39. [doi.org/10.1016/S0034-6667\(02\)00075-1](https://doi.org/10.1016/S0034-6667(02)00075-1).
- van der Kaars, S., De Deckker, P., Gingele, F.X. (2006). A 100,000 year record of annual and seasonal rainfall and temperature for northwestern Australia based on a marine pollen record. *Journal of Quaternary Research*, 21, 879-889. [doi.org/10.1002/jqs.1010](https://doi.org/10.1002/jqs.1010).
- Yokoyama, Y., et al. (2018). Rapid glaciation and a two-step sea level plunge into the Last Glacial Maximum. *Nature* [doi.org/10.1038/s41586-018-0335-4](https://doi.org/10.1038/s41586-018-0335-4). Doi.org/ 10.1038/s41586-018-0335-4.